A simulation study of SUGRA and GMSB signatures in the ATLAS detector at LHC, CERN

Thesis submitted to the cand. scient. degree in experimental particle physics

Halvor Kippe,
Department of Physics, University of Oslo

May 2001

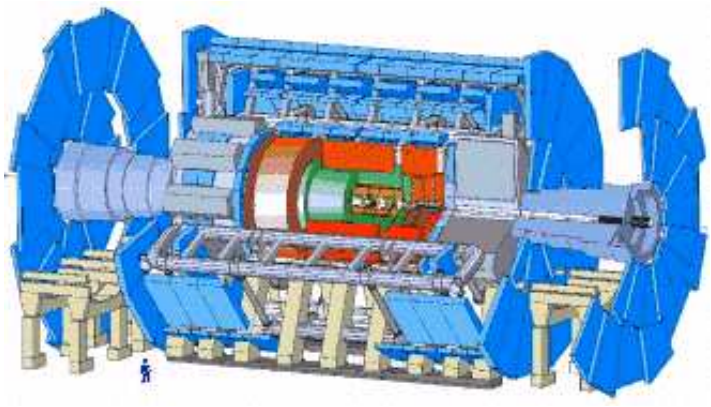

Abstract

The main purpose of this thesis is to study possible signatures of supersymmetric decays in the ATLAS detector at the LHC (currently under construction at CERN), covering a wide parameter space of two supersymmetric GUT models. The analysis is based upon Monte Carlo simulated data, assuming the SUGRA and GMSB models. The focus will be mainly on SUGRA. A fast simulation of the ATLAS detector is used.

Acknowledgements

Several people have been helpful, supportive and patient during the time I have spent working on this thesis. Especially my supervisor Steinar Stapnes, who has thoroughly gone through this paper in all its phases, correcting errors at all levels of detail. And also Ole Myhren Røhne deserves to be mentioned, since he was the one who taught me how to get started with the software, and because he, even a long time after he finished his deployment here in Oslo, helped me out of several problems that appeared during the process of building up a consistent analysis. Also in the last part of the thesis he has contributed with corrections and comments. Trond Myklebust has been the one to which I have put my trust when the computers have been unwilling to cooperate. His knowledge has been invaluable, and his quick response in numerous “crisis situations” has made it possible for me to get a sense of continuity in my work, not having to “call it a day” whenever a computer has crashed, waiting for external technical support. Børge Kile Gjelsten has been helpful with methods concerning preselection cuts to reduce the SM QCD background production cross section.

All the other members of the research group for experimental particle physics at the Physics Department, University of Oslo, and some from the theory group as well, have contributed to this thesis through valuable conversations and inspiring talks, regarding both theoretical and technical issues.

Contents

1.0 Introduction

1.1 CERN

The European Centre for Nuclear Research, CERN, is the world's largest particle physics laboratory. Scientists from all of Europe and many other countries are doing frontier research in virtually every area within high energy physics (and a few other areas as well).

CERN is originally an abbreviation of Conseil Européen pour la Recherche Nucléaire. It had a provisional council sited in Amsterdam. CERN took its form as the European Organization for Nuclear Research the 29. of September 1954 (but kept its now rather meaningless abbreviation). The French physicist Luis de Broglie made the initial proposal at the European Cultural Conference in Lausanne in 1949. At first there were only twelve member states: The Federal Republic of Germany, Belgium, Denmark, France, Greece, Italy, Norway, The Netherlands, United Kingdom, Sweden, Switzerland and Yugoslavia. Today there are twenty member states. Yugoslavia is not a member any more, but Austria, Spain, Portugal, Finland, Poland, Hungary, the Czech and Slovak Republics and Bulgaria have all joined in. In addition to that several so-called observer states are also present at CERN. These are Israel, Japan, the Russian Federation, Turkey, the United States of America, the European Commission and Unesco. If one takes into account all the non-member countries that are involved in CERN programs, it adds up to a total of more than 6500 scientists (about half of all particle physicists in the world), representing more than 500 universities from over 80 nations, using the laboratories at CERN.

During the years, several great achievements have been made by various CERN experiments [1]. These are the most famous ones:

- Discoveries of the massive vector bosons W^+, W^- and Z^0 in the UA1 and UA2 detectors at the SPS in 1983
- Neutral currents "seen" in the Gargamelle bubble chamber detector in 1973
- Invention of multiwire-proportional chambers and drift chambers (both by Georges Charpak in 1968)
- Production of antimatter hydrogen atoms (at LEAR in 1995)
- The LEP experiment's strong evidence that there are only three "flavour" families of matter (1989-1995)

Throughout the years people have found many ways of taking advantage of the various new technologies that have been developed at CERN. Some of the most important spin-off effects are mentioned below:

- Hypertext
- Other web protocols
- Accelerator-based nuclear power plant technology
- Cancer therapy
- Medical and industrial imaging
- Radiation processing
- Advanced electronics
- Superconducting magnets technology (cryogenics)
- Measuring instruments
- New manufacturing processes
- Food preservation techniques
- Destruction of toxic and radioactive products

1.2 The Large Hadron Collider (LHC)

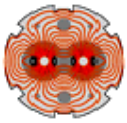

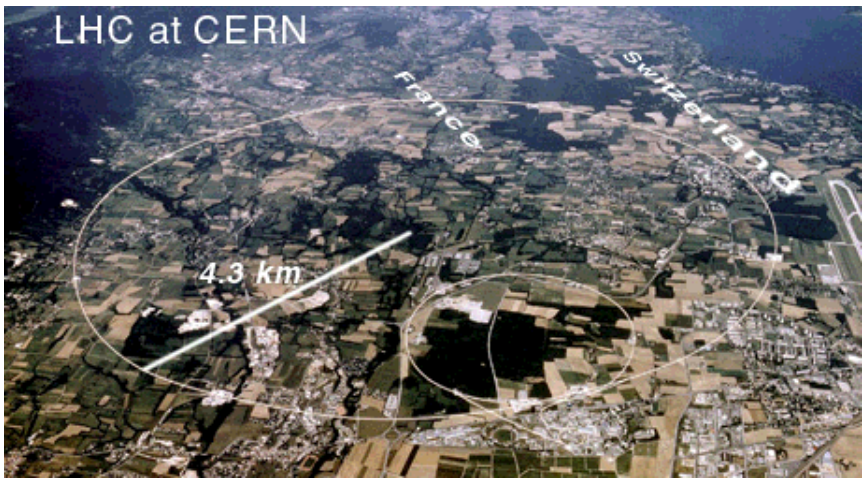

Figure 1.1: The LHC area.

The Large Hadron Collider is a $\sqrt{s}$ = 14 TeV proton-proton collider currently under construction in the 27 km circumference LEP tunnel in the Franco-Swiss border area west of Geneva. It is expected to be a “discovery machine” more than a precision measurements machine (as LEP). Hadron physics is generally more difficult to do with high precision than lepton physics, but higher energies are accessible due to less synchrotron radiation losses (because all hadrons have more mass per unit electric charge than electrons). The construction and exploitation of the LHC will be the major challenge for CERN the next couple of decades. It is designed to reach a luminosity of L = 10^{34} cm^{-2} s^{-1}, corresponding to a beam current of 0.53 A and $\int L\,dt \sim 100$ fb^{-1} per year. At such a high luminosity each beam pipe will contain 2835 bunches of 10^{11} particles. One LHC experiment at maximum luminosity will generate data at a rate about equal to everyone on Earth simultaneously making 20 telephone calls each [8]. Very rare processes (with small cross sections) are thus accessible within reasonable runtime.

LHC will become the largest cryogenic facility in the world, because of the approximately 1300 superconducting dipole magnets, operating at 1.9 K.

There are five major LHC experiments: ATLAS (**A** **T**oroidal **L**HC **A**pparatu**S** - general purpose), CMS (**C**ompact **M**uon **S**olenoid - general purpose), ALICE (**A** **L**arge **I**on **C**ollider **E**xperiment), TOTEM (an experiment to measure total cross section, elastic scattering and diffraction dissociation at the LHC) and LHC-B (to study CP violation in B-meson decays) [3].

The first run is scheduled to start in 2006.

2.0 The ATLAS Detector

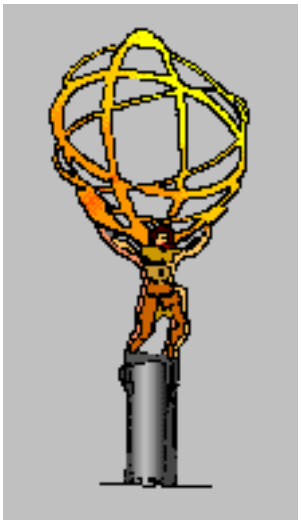

ATLAS (**A** **T**oroidal **L**HC **A**pparatu**S)** is one of the two multipurpose detectors at the LHC. The abbreviation is quite suggestive, as reflected by its impressing dimensions [4]:

- Length: 40 m
- Radius: 10 m
- Weight: 7000 tons

The inner detector (figure 2.1) consists of a high resolution silicon pixel detector and a silicon strip tracker (SCT: SemiConductor Tracker), surrounded by a straw tube Transition Radiation Tracker (TRT). Its outer radius is 115 cm, the length is 7 m.

The purpose of the SCT is to make important contributions to measurements of the momentum of a charged track (see below), impact parameter, vertex position and pattern recognition by making eight precision measurements per track. Compared to previous generations of silicon microstrip detectors, the surface area of this SCT will be about one order of magnitude larger. The total area of silicon detectors in ATLAS will be about 50 m^2, with more than 6 million readout channels ($4088 \cdot 128 \cdot 12$). The SCT spatial resolution is expected to be 16 μm in the transverse plane and 580 μm in the direction of the beam pipe (z-axis/longitudinal direction). The η coverage of the ID is ± 2.5.[1]

One of the most difficult tasks of particle detection is to identify b-jets. Tagging of b- and τ–jets is made in the pixel detector (both bottom quarks and τ leptons have decay lengths in the mm region). If a b-quark with $p_T > 5$ GeV is found within a $\Delta R < 0.2$[2]

1. For a definition of pseudorapidity, see equations 6.1a and 6.1b.
2. See equation 6.0 for a definition of separation ΔR.

cone from a jet, the jet is labelled a b-jet. The jet must also have $|\eta| < 2.5$. The assumed ATLAS b-tagging efficiency (averaged over p_T) is only 60% in the software used in this thesis (that is what is expected at low luminosity - at high luminosity it is expected to decrease to 50%), while the efficiency of rejecting non-b-jets is believed to be about 99%. B-tagging is of great importance when looking for hadronic Higgs decays, because Higgs bosons will preferentially decay to the heaviest particles available.

General tracking and electron identification by detection of transition photons at extremely high rates is the main objective of the straw tube TRT. The gas content of the straws is: 70% Xe, 20% CF_4 and 10% CO_2, with a total volume of 3 m^3. There will be 50 000 straws in the barrel and 320 000 radial straws in the endcaps, with a total of 420 000 electronic channels (the barrel straws have readout channels in both ends). Each straw is 4 mm in diameter, with a 40 μm gold-plated W-Re wire. Drift-time measurements are provided in each channel, which will give a spatial resolution of 170 μm per straw. The straws will operate with two independent tresholds, making it possible to discriminate signals that pass either the low (tracking hits) or the high treshold (transition radiation hits).

Winded around the whole ID construction there will be a 2 Tesla superconducting solenoid, to create a uniform B-field. By measuring a charged particle's radius of curvature in this magnetic field, we will be able to find its momentum (mass spectroscopy). Together with information on the energy deposition in the calorimeters, this will allow us to identify the particle in the charged track.

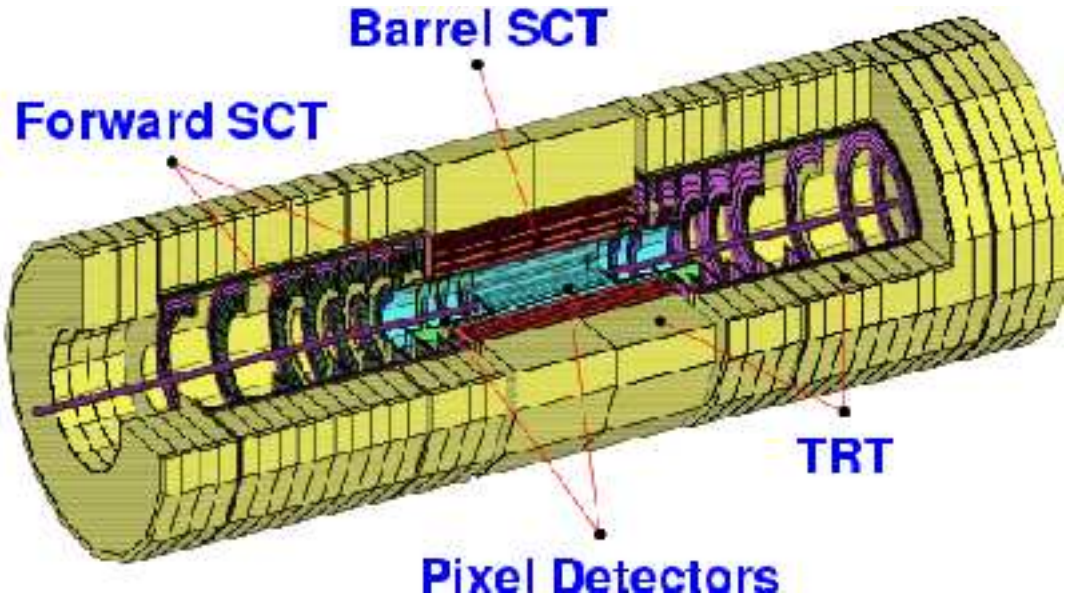

Figure 2.1: ATLAS Inner Detector [8].

Electron and photon identification and energy and position measurements are made (in combination with information from the ID) in the lead Liquid Argon (LAr) electromagnetic calorimeters (EMCALs). The whole EMCAL construction has an accordion geometry; "zig-zag" Kapton electrodes in the barrel and two endcaps, covering the pseudorapidity regions $|\eta|<1.475$ (barrel) and $1.375 < |\eta| < 3.2$ (endcaps).

Jet reconstruction (position and energy) will be carried out in the hadronic calorimeters (HCALs), as well as in the EMCALs. The HCALs will include a barrel HCAL, two endcaps and a forward calorimeter (FCAL). The barrel HCAL will consist of three cylinder sectors, where a sampling technique with plastic scintillator tiles in an iron absorber will be used. In the endcaps and in the FCAL larger radiation resistance is necessary. For that reason the radiation-hard LAr technology will be used there. The endcap HCALs will be made of parallel-plate geometry copper LAr detectors, while the hadronic FCALs will be dense LAr calorimeters with rod-shaped electrodes in tungsten matrices. The FCAL coverage will be $3.1 < |\eta| < 4.9$, while the region $|\eta| < 3.2$ is covered by the hadronic endcaps. The scintillating tiles in the barrel will operate in the range $|\eta| < 1.7$.

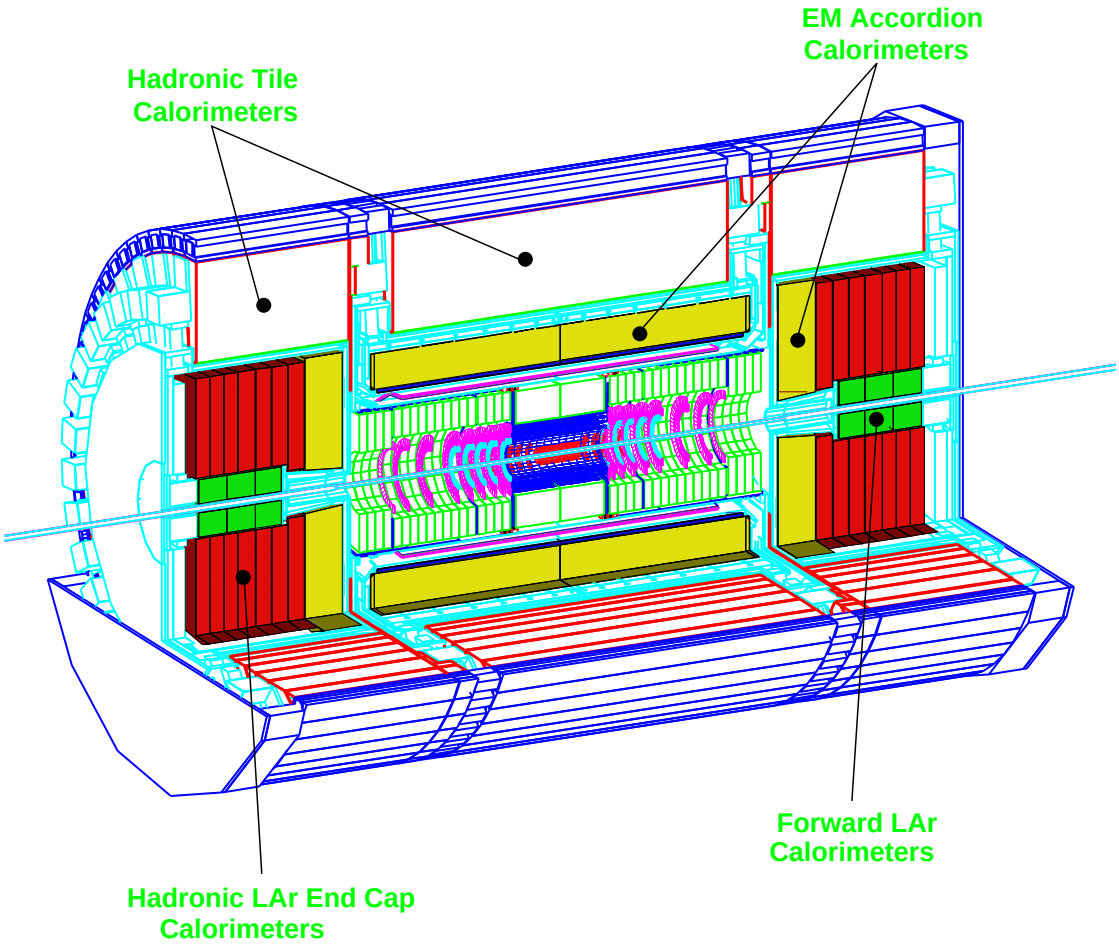

Figure 2.2: Calorimeter layout [4].

Outside the calorimetry and the muon chambers there will be eight large superconducting toroids of air-core independent coils encapsulating the barrel (3.9 T peak value) (see figure 2.5), and two endcap toroids (4.1 T peak value) to generate the magnetic fields for muon spectroscopy. The muon chambers will thus provide a high resolution,

large acceptance and robust stand-alone muon spectrometer [16]. Multiple scattering effects are minimised by the large volume and great bending power of the magnetic fields. Three stations (cylindrical layers) of high precision tracking chambers provide ATLAS with excellent muon momentum resolution. The precision track measurements will in most of the pseudorapidity range be carried out by monitored drift tubes (MDTs), except at large η and near the interaction point, where higher granularity is necessary. Here cathode strip multiwire proportional chambers (CSCs) will be installed, because they are better at withstanding the higher signal rate and larger background. The muon trigger chambers constitute the last two muon chamber technologies to be employed in ATLAS. Resistive plate chambers (RPCs) will be mounted on the barrel in three stations, covering the barrel trigger function, while in the endcaps the trigger function is provided by three stations of thin gap chambers (TGCs).

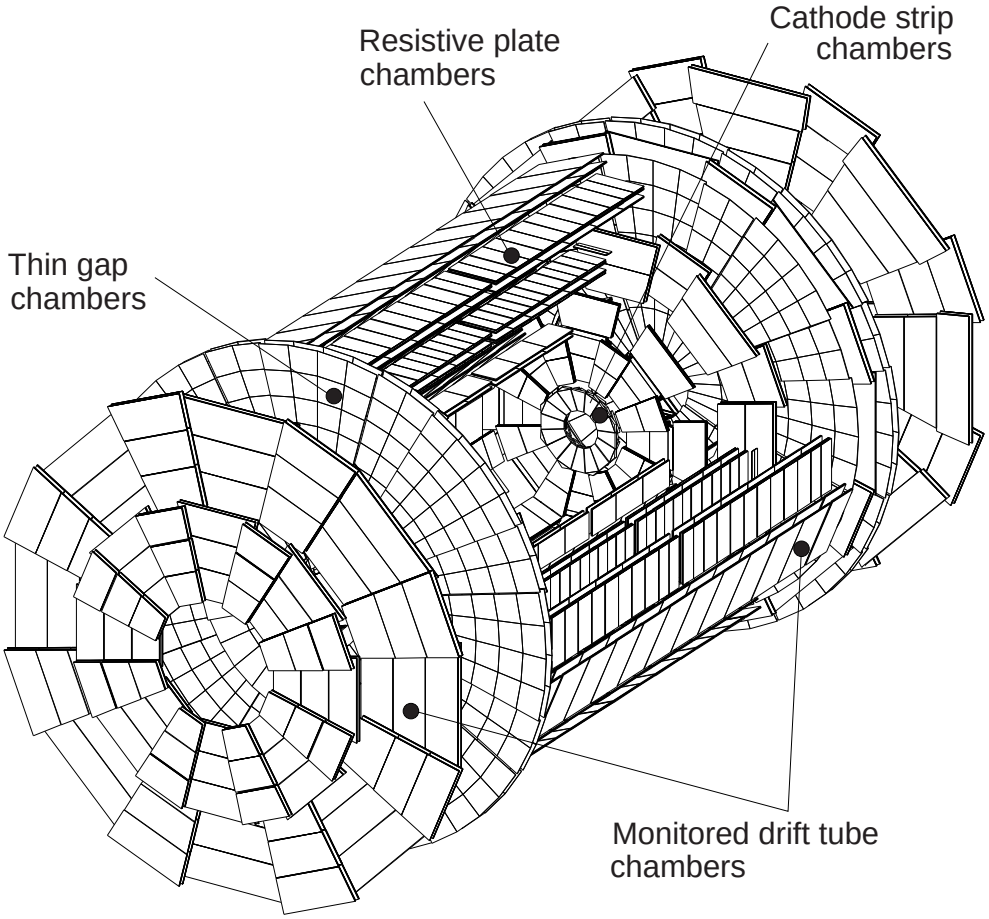

Figure 2.3: Muon chamber layout [4].

The trigger system consists of level 1 (LVL1), level 2 (LVL2) and an Event Filter (EF), reducing the data rate from 10^9 Hz initial rate ($L = 10^{34}$ $cm^{-2}s^{-1}$) to about 100 Hz final rate, corresponding to a rejection factor of 10^7 against minimum bias events (events with low momentum transfer). The LVL1 discrimination decision is based on high p_T

muon identification in the muon trigger chambers, high p_T electrons and photons, jets, τ-leptons decaying into hadrons, large missing and total transverse energy in the calorimeters. The exact selection criteria may be reprogrammed even at LVL1, making it very flexible for the versatile tasks of the ATLAS detector. The quality of the LVL1 trigger is of enormous importance, considering it has to make a decision every 25 ns at maximum luminosity. The physical response time both in the muon trigger system as well as in the calorimeter trigger makes this very difficult to cope with. The expected target latency is 2.0 μs.

The LVL2 trigger is expected to reduce the rate from 75-100 kHz to ~ 1 kHz, having a latency time in the range 1-10 ms. It will make its decisions based on information on position (η and ϕ), p_T, total and missing E_T of the candidate events from the LVL trigger. Applying a 'region-of-interest' mechanism allows the LVL2 trigger to make its decision with use of only a few percent of the total event data. It will, nevertheless, have access to transition radiation signature information from the ID, full granularity information from the calorimeters and precision muon chambers information.

To reach the final rate of about 100 Hz, an Event Filter (EF) will be installed to make the final online physics selection. It will use offline algorithms, adapted to the online environment, as well as information on alignment and calibration and a magnetic field map.

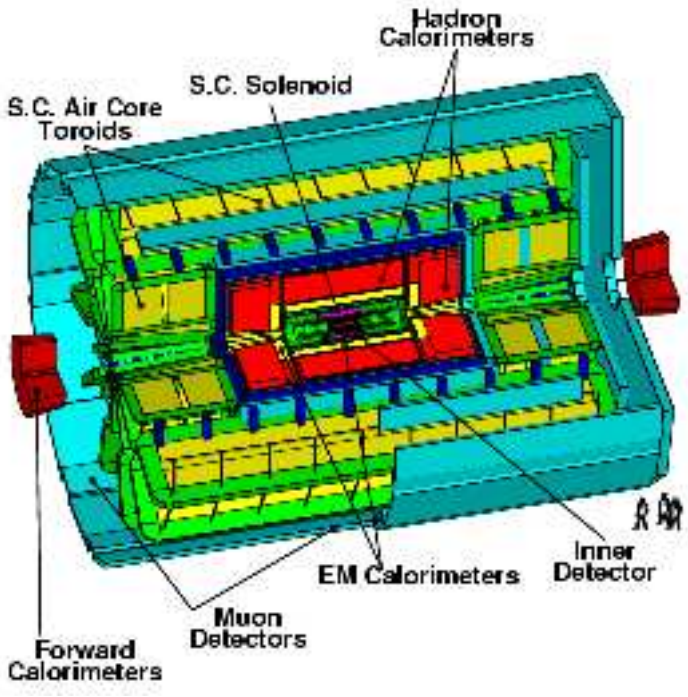

Figure 2.4: Schematic diagram of the ATLAS detector [12].

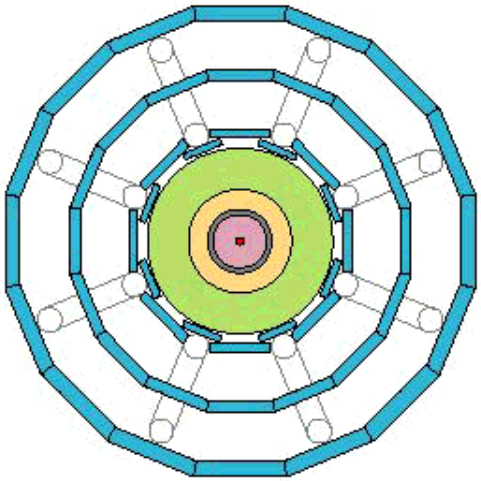

Figure 2.5: Endview of ATLAS [8].

3.0 Physics

LHC is an extremely ambitious project. Virtually everyone who is involved in it is expecting new physics (that is: phenomena which cannot be explained in the Standard Model) to occur within the reach of LHC's capacity regarding energy level, luminosity and precision of measurements. The following subchapters describe some of the fields that might be explored at the LHC.

3.1 SM Studies

The high luminosity, centre of mass energy and level of precision in the detectors allow for detailed measurements of several Standard Model parameters, such as the W and t-mass, triple and quadruple gauge couplings (figure 3.1 and 3.2) and precise CKM-matrix elements determination. The latter will increase the level of detailed knowledge on the mechanism of CP violation.

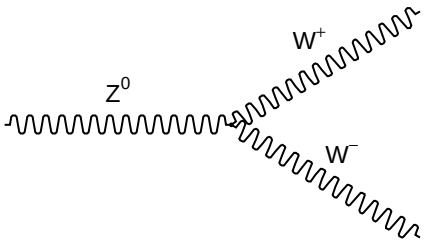

Figure 3.1: W boson pair production.

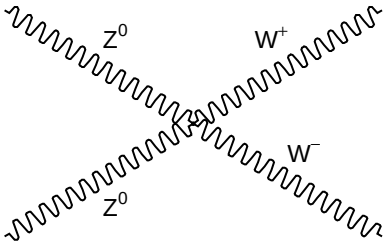

Figure 3.2: Coupling between two Z bosons and two W bosons.

3.2 Electroweak Symmetry Breaking

The electroweak $U(1) \times SU(2)$ symmetry must be broken to provide massive vector-bosons (or any other massive SM particles). It is either broken spontaneously (as in Higgs mechanism scenarios) or dynamically (as in technicolour models). Either opportunity predicts new physics to occur at $\sqrt{s} \sim 1$ TeV. This is one of the strongest arguments to build the LHC.

Standard Model Higgs searches will be conducted mainly in these channels:

$$gg \to H, q\bar{q} \to WH, gg \to t\bar{t}H, gg \to b\bar{b}H, qq \to qqH\,;\, H \to f\bar{f}, \gamma\gamma$$

$f\bar{f}$ means any fermion/antifermion pair. The heaviest fermions kinematically available have the largest branching ratios, because the Higgs field couples to mass. In most scenarios the Higgs boson is too light for top quark decays. Many particle physicists expect the Higgs boson to be discovered at the Tevatron (Fermilab, USA), due to the small excess of signal versus background for a Higgs mass of about 115 GeV hypothesis in the final runs of LEP2 at CERN [20]. The 95% confidence exclusion limit is now as high as 113.5 GeV.

3.3 What Is Wrong With The Standard Model?

The SM is considered insufficient in a number of ways, and is by most theoreticians considered an efficient low energy approach to more fundamental theories. These are a few of the problems which the SM has left unanswered:

- The Hierarchy Problem: Loop corrections to the Higgs mass is of the order the energy scale up to which the SM is considered 'valid'. This mixing of energy scales (the electroweak and the GUT scale) is called The Hierarchy Problem. The divergence in the perturbation series is quadratic in the cutoff Λ (the scale at which new physics should appear), while other divergences in the SM are only proportional to $\log \Lambda$. Finetuning is a very unpopular candidate solution to The Hierarchy Problem. It requires a finetuning of a parameter to 34 significant digits to make the Higgs mass compatible with present precision electroweak measurements. More explicitly, it says that the difference of two squared massed of order 10^{15} GeV[1] each should be of order the mass of the W bosons squared. In that case one keeps the Higgs boson mass at a reasonable level. That is also called 'The Unnaturalness Problem' (because such finetuning does not seem very natural).
- The SM contains 19 unpredicted parameters, which is considered unaestethic by many theoreticians.
- How do we explain the matter-antimatter asymmetry in the universe? The present understanding of CP violation suggests that this has something to do with the excess of matter to antimatter, but does probably not fully account for it.

1. The convention ħ = c = 1 is used throughout this document

- Where did the three generations of fermions come from? And what is the origin of the mixing between them, parameterised by the CKM matrix? The SM gives no answers to this.
- Why is there such a thing as CP violation?
- A history of substructures: How can we be so sure that quarks and leptons do not possess inner structures? It is a good tradition to find smaller parts of what was believed to be elementary. Just think about the atom.
- What is really the nature of QCD confinement?
- A plot of coupling strength versus energy (figure 3.5) suggests a possibility that the electromagnetic, the weak and the strong coupling constants meet each other at some high energy scale (of order 10^{15} GeV or, as suggested by recent developments in higher dimensional string theories; maybe as low as around 1 TeV). In that case, one cannot distinguish between the forces, and one should describe the three forces as one. The LEP experiment told us that the coupling constants do not merge within the SM, but it is allowed in SUSY models (figure 3.5).

3.4 SM Extensions

Instead of rejecting the Standard Model in favour of some new model, valid at higher energies, it is tempting to make additions to it, attempting to explain some of the most important unanswered questions. The following is a short presentation of some of the proposed SM extensions.

3.4.1 Technicolour Models

Technicolour is an alternative way to break electroweak symmetry (dynamically, not spontaneously as in Higgs models). Introducing this universal $SU(3)$ interaction at high energies allows us to let SM particles have mass without violating the gauge invariance of the Lagrangian. Such models imply that there should be no fundamental bosons. They also predict the existence of technipions, techni-ρ etc. The fundamental building block is the techniquark. Because there are no scalars, there is no Hierarchy Problem related to boson masses (see 3.3). The vector bosons become technimesons, consisting of lefthanded techniquarks.

3.4.2 MSSMs

MSSMs are **M**inimal **S**upersymmetric **E**xtensions of the **S**tandard **M**odel. That means one does not introduce more new particles than what is necessary to call the theory supersymmetric (see 3.6). So all SM particles get their “sparticle” partners and another doublet is added to the Higgs sector to avoid triangle anomalies when the fermionic Higgsinos are added to the spectrum and to give masses to up and down type quarks separately. So the MSSM Higgs particles are as follows:

- Two charged scalars H^+ and H^-
- One heavy, neutral scalar H^0

- One neutral pseudoscalar A^0
- One light, neutral scalar h^0

An unconstrained, naive MSSM model contains 124 independent parameters. SUGRA (3.6.3) and GMSB (3.6.4) are strongly constrained MSSM models that also say something about the particle spectrum at the unification scale and how SUSY is broken.

The perhaps strongest single, parameter independent prediction of constrained MSSMs, is that the lightest Higgs mass should be within 120 ± 10 GeV, taking loop corrections into account [18].

3.4.3 Anomalous TGCs and QGCs

Triple and quadruple gauge couplings that violate conservation of weak isospin:

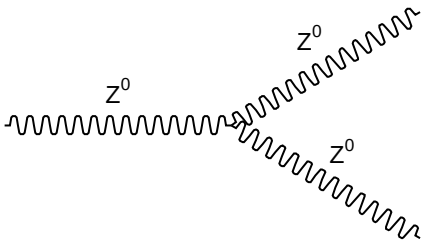

Figure 3.3: Three Z^0 coupling.

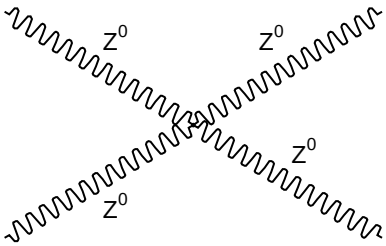

Figure 3.4: Four Z^0 coupling.

Such processes are not allowed within the SM, and would thus be good evidence for physics beyond the SM.

3.4.4 New gaugebosons

Higher dimensional string theories often predict the existence of heavier “cousins” of the vector bosons, namely W’ and Z’. These might appear in LHC experiments.

3.4.5 Compositeness of quarks and/or leptons

There might be an inner structure at a scale Λ, where valence quark scattering dominates in hadrons. These particles are called subquarks, preons or rishons. The signatures are more hard jets and more isotrope angular distribution of dijets than expected from QCD.

3.4.6 Leptoquarks

The idea of leptoquarks is conceived from the fact that fermions in the SM show a symmetry between leptons and quarks, namely that both are organised into three generations of doublets [14]. That might lead us to imagine that there may exist a coupling between them, mediated by a new kind of boson. Leptoquarks appear naturally in GUT models (3.5), where quarks and leptons share multiplets. Their characteristics are believed to be:

- Non-zero lepton and baryon numbers
- Fractional charge
- QCD colour
- Scalar and/or vector transformation properties
- Either very massive or couple only within one generation (or else we would have seen processes like $\pi^0 \to \mu e$, $\pi \to e\nu$, $K \to \pi\nu\nu$ and $K \to e\nu$)

Leptoquark production: $q + g \to LQ + l$

Leptoquark pair production: $g + g \to LQ + LQ$

Allowing quarks to decay into leptons leads to proton decay at the weak scale.

3.5 GUT Models

3.5.1 What is a GUT Model?

GUT is an abbreviation of ‘Great Unified Theory’. A GUT model aims to describe three of the four fundamental forces in the same framework, and by the same parameters. These forces are the electromagnetic, the weak and the strong nuclear force. Gravity is left out. The three coupling constants will merge into one common coupling at the so-called GUT scale $M_{GUT} \sim 10^{15}$-10^{16} GeV (figure 3.5). All the involved fields are put into one common multiplet. This leads to the existence of leptoquarks (3.4.6).

GUT models have an electromagnetic charge operator as one of the group generators. That means the electromagnetic charge is automatically quantised, which is a great improvement from the SM U(1) Maxwell theory, in which charges are continous.

Perhaps the biggest problem in most GUT models is that they predict that massive magnetic monopoles should be the dominant type of non-relativistic matter at high

energies, which implies that the universe at today's energy scale also should be filled with magnetic monopoles, which is clearly not the case. This problem may be solved in cosmology by thermal inflation. Not only GUT models have this problem. In fact; all attempts to embed the SM U(1) group into a non-abelian symmetry group that is broken spontaneously at high energies, will give rise to a monopole problem [9].

Another problem in GUT models is, as in all leptoquark scenarios, that proton decay at the weak scale is a natural consequence.

Most common group structures are SU(5), SO(10) and E_6. SUSY GUTs are the most promising candidates for reasons discussed below.

3.5.2 Why SUSY GUTs?

First of all, radiative electroweak (EW) symmetry breaking appears naturally in gravity mediated and gauge mediated SUSY breaking models, because one of the diagonal Higgs squared mass parameters is driven negative by the renormalization group evolution. Secondly, if SUSY is conserved at the electroweak energy scale, it provides not only a solution to The Hierarchy Problem given under 3.3 (see 3.6 for a further explanation), it also allows us to cancel the cosmological constant in some corners of the parameter space (because the potential of the theory is not positive definite). If R-parity is conserved (see 3.6.2), any of the supersymmetric models requires a stable LSP (Lightest SUSY Particle). Then the LSP is a candidate for cold dark missing matter in galaxies in some parts of the parameter space.

As mentioned in the end of 3.3, it seems like we need an extended particle spectrum to make the fundamental couplings unify in a point. The SUSY particle spectrum might make this possible, as illustrated in figure 3.5, provided that the masses are of the order 1 TeV.

Some of the (infinite number of) SUSY models reduce the number of arbitrary parameters in the theory significantly, based on quite general assumptions. SUSY is also the only known reasonable way to incorporate gravity in a common quantum theory of all interactions (superstring theories are supersymmetric). So even if SUSY is not conserved at the GUT scale, it should be so at the string or Planck scale for a complete unification of all four forces.

SUSY GUT models are divided into different classes, depending on which way the symmetry breaking is implemented. SUSY breaking is usually transmitted from a hidden sector of particles, in which SUSY is already broken. In SUGRA (SUper GRAvity) models, gravity is the mechanism responsible for the breaking, while in GMSB (Gauge Mediated SUSY Breaking) models, ordinary $U(1) \times SU(2) \times SU(3)$ gauge interactions communicate the breaking from the hidden to the physical sector. Recently, so-called AMSBs (Anomaly Mediated SUSY Breaking GUT models [11]) have also appeared, offering yet another mechanism for transmitting SUSY breaking to the physical sector. SUGRA and GMSB will be discussed in more detail in 3.6.3, 3.6.4 as well as in the analysis chapters (6 and 7).

Identification of the Lightest Supersymmetric Particle (LSP) in ATLAS may exclude either one of the two mentioned models. The GMSB model predicts the LSP to be the gravitino ($\tilde{G}$), while in SUGRA the LSP is the lightest neutralino ($\tilde{\chi}_1^0$).

Supergroups are orthogonal to gauge groups, so the unification gauge group structure is not constrained neither for SUGRA nor GMSB. Any of the groups mentioned in 3.5.1 should in principle be applicable for both SUGRA and GMSB models.

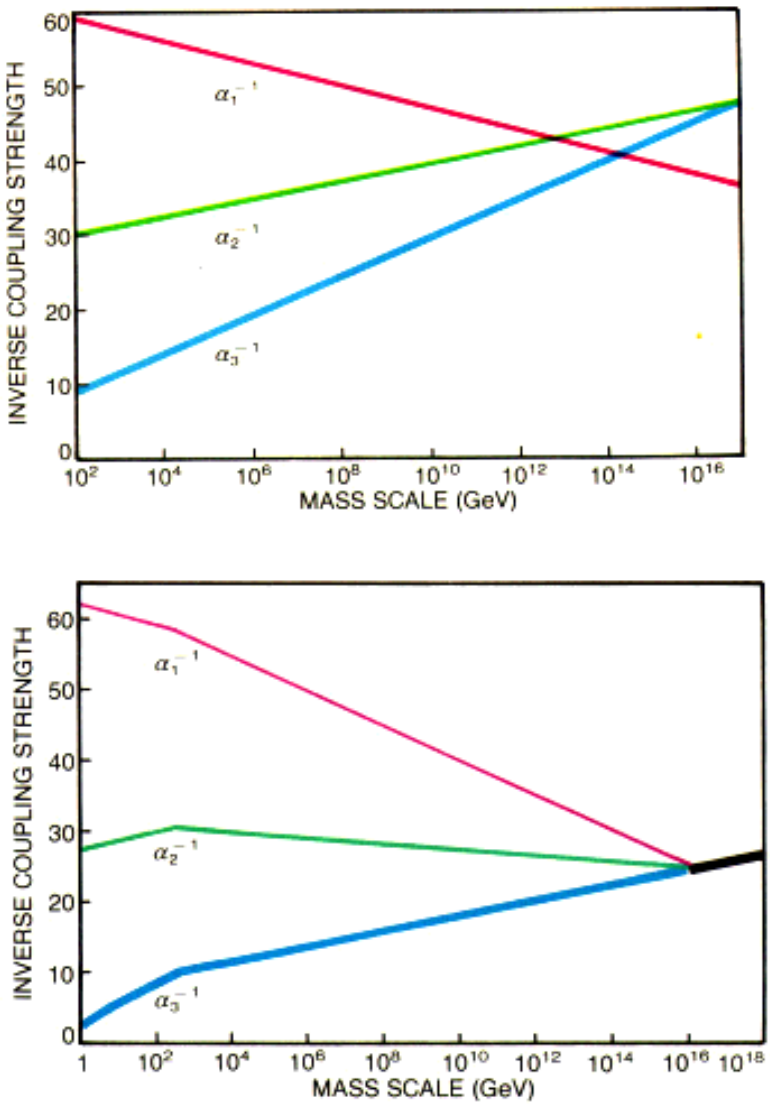

Figure 3.5: SM coupling constants merging at GUT scale. The upper part is without SUSY and the lower part is with SUSY [17].

3.6 SUSY

Supersymmetry means phenomenologically that for every boson (fermion) in the model, there exists a fermion (boson) partner with exactly the same mass and quantum numbers, except that the spin is shifted by $\pm 1/2$ units.

In SUSY scenarios all SM fields are replaced by chiral superfields, in which both the SM particles and the SUSY partners are contained.

All the supersymmetric partners of the original bosons are called the same as the boson, only that the suffix '-on' is replaced by '-ino'. The superpartner of the gluon is for instance called a gluino. The superpartners of the fermions are called the same as their 'cousins', except that one puts an 's' in front, so that quark partners are squarks and lepton partners are sleptons. This symmetry is obviously not conserved at any observed scale, since we have yet to see in any experiment an integer spin selectron with a mass of roughly 511 keV.

More theoretically, one says that supergroups (or mastergroups) are the only possible, non-trivial expansion of the Poincaré group, meaning that SUSY is required in a quantum theory of gravity.

By calculation of loop corrections to a SM particle mass, fermion and boson loops have opposite sign contributions. That means that when one introduces superpartners to all SM particles, each term in the perturbation series will be cancelled by an opposite sign term due to the new superpartners. In that way we get rid of the quadratic divergences in the boson mass calculations. That is considered a very attractive way to solve the Hierarchy Problem given under 3.3. It only requires $\left|m^2_{sparticle} - m^2_{particle}\right|^2 \leq 1\ \text{TeV}^2$ [19].

MSSMs are perhaps the most popular extensions of the SM. What separates the different MSSMs is the soft SUSY breaking term in the Lagrangian. There is no general argument in the theory that tells us what kind of SUSY breaking we have. It has to be introduced in the Lagrangian "by hand". The nature of this soft SUSY breaking term (which of course must be gauge invariant) defines what kind of MSSM we have (for instance SUGRA or GMSB).

3.6.1 The minimal SUSY particle spectrum

At energies where supersymmetry and electroweak symmetry are conserved (radiative EW symmetry breaking follows from the breaking of SUSY), these particles come in addition to the SM spectrum:

- Three generations spin zero squark singlets ($\tilde{u}_R{}^*$, $\tilde{d}_R{}^*$, …) and doublets ($\tilde{Q} = (\tilde{u}_L, \tilde{d}_L)$, …).
- Three generations spin zero slepton singlets ($\tilde{e}_R{}^*$, …) and doublets ($\tilde{L} = (\tilde{\nu}_e, \tilde{e}_L)$, …).

- Two spin $1/2$ Higgsino doublets ($\tilde{H}_u{}^+$, $\tilde{H}_u{}^0$, $\tilde{H}_d{}^0$ and $\tilde{H}_d{}^-$).
- Three spin $1/2$ winos ($\tilde{W}^0$, $\tilde{W}^-$ and $\tilde{W}^+$).
- One spin $1/2$ bino ($\tilde{B}$) and eight gluinos ($\tilde{g}$).

When the electroweak symmetry is broken, the gauginos (winos and binos) mix with the Higgsinos to form four neutralinos ($\tilde{\chi}_i^0$) and two charginos ($\tilde{\chi}_i^{\pm}$). This mixing is determined by tan β and μ (defined in chapter six) and is motivated by the argument that particles with the same quantum numbers in general mix. There is no reason to believe that the so-called gauge eigenstates (winos, binos and Higgsinos) are simultaneously mass eigenstates.

The four extra bosons given in 3.4.2 are added to the Higgs sector.

3.6.2 R-Parity

R-parity is a proposed multiplicative symmetry that involves both lepton number, baryon number and spin of a particle: $R = (-1)^{L+3B+2J}$

Other, equivalent definitions are often used.

R = 1 for particles and R = -1 for sparticles means that sparticles must be produced in pairs if the symmetry is to be conserved. If it is not an exact symmetry, baryon or lepton numbers might not be conserved, which in turn leads to weak-scale proton decay, which would have a rather disastrous impact on the universe and is in contradiction with experiments.

We do not know whether it is a fundamental symmetry or not, although it is assumed to be so in most analyses. Some scenarios, though, allow weak R-violations by the LSP only. Then the effect of proton decay would be less dramatic, but still measurable.

The concept is introduced mainly to reduce the enormous MSSM parameter space by eliminating some clearly non-physical parts of it. It does not follow naturally from general SUSY arguments.

3.6.3 SUGRA

In this constrained MSSM supersymmetry breaking is transmitted from a hidden sector to the physical sector by gravitational interactions. SUSY is broken explicitly in the total Lagrangian. The basic assumption is that at GUT level all scalars (squarks, sleptons and Higgs bosons) share the same mass (m_0), and all fermions (SM fermions, Higgsinos and gauginos) have the mass $m_{1/2}$. All the Higgs-sfermion-sfermion couplings have the common value A_0. These assumptions come from the fact that gravity is universal.

3.6.4 GMSB

Gauge Mediated Supersymmetry Breaking model is an alternative to SUGRA, where SUSY breaking is transmitted by a messenger that is a new gauge particle. The gravitino gets its mass only from gravitational interactions at the Planck scale, so it will be the LSP (some times lighter than 1 GeV).

More details about both models will appear in chapter 6 and 7.

3.6.5 Searches for Supersymmetric Particles

In all minimal extensions of the Standard Model (MSSMs), there are two Higgs doublets (explained in 3.4.2). Consequently, looking for supersymmetry means searching for signatures for SUSY Higgs decays, as well as direct searches for sparticle decays.[1]

Assuming that all SUSY particle masses are heavy compared to all Higgs particle masses, there are several channels with substantial Higgs discovery potential:

$h/H/A \rightarrow \gamma\gamma$

$h/H/A \rightarrow f\bar{f}$

$H \rightarrow ZZ \rightarrow llll$

$A \rightarrow Zh \rightarrow f\bar{f}f\bar{f},\ f\bar{f}\gamma\gamma$

$H \rightarrow hh \rightarrow f\bar{f}f\bar{f},\ f\bar{f}\gamma\gamma$

Signatures for supersymmetric particles are:

1. Missing energy in the transverse plane (E_T) from the LSP escaping detection.

$E_T = \sqrt{p_x^2 + p_y^2}$ (z-axis parallel to the beam pipe)

2. Large p_T-jets from cascade decays.
3. Leptons from chargino and neutralino decays.
4. B-production from decays of $\tilde{t}$, $\tilde{b}$ and Higgs-bosons.

3.6.6 Disadvantages of SUSY Models

Not everything is beautiful, simple and straight-forward in a supersymmetric world. Here are some of the most important objections to the concept:

- No evidence: We have so far no experimental reasons to believe in supersymmetry (although the results in figure 3.5 fit well to an MSSM).

1. An extended Higgs sector is not unique for SUSY models, but occurs in other models as well.

- Nasty particle spectrum: SUSY more than doubles the number of particles compared to the Standard Model.
- Unpleasant number of independent parameters: The naive, unconstrained MSSM leaves us with 124 unpredicted, independent parameters. Hardly an improvement from the SM (containing only nineteen).
- Violation of both lepton numbers and baryon numbers is a natural consequence of SUSY. To avoid this, one has to introduce yet another symmetry (R-parity).

4.0 SUSY Searches

The SUSY particle production cross section is dominated by pair production of gluinos and squarks. They decay mainly into a light chargino and two neutralinos. Eventually an LSP is created at the bottom of the decay chain (R-parity conservation is assumed, see 3.6.2), so that a general SUSY event always contains some missing energy due to the escape of the LSP, multiple jets and leptons.

Gluinos are expected to be only produced in pairs (to avoid R-parity violation). Because they are Majorana fermions, which means they are their own antiparticles, gluinos have equal branching ratios into l^+X (X = undefined hadrons) and l^-X, so another inclusive SUSY signature is to look for isolated, likesign dileptons.

Inclusive measurements may tell us whether we have seen SUSY events or not, but to investigate SUSY further, and to figure out how it is broken, we should study exclusive signatures as well. That means looking at certain final states, trying to reconstruct masses partially. Because of the escape of the LSP, it is impossible to fully reconstruct all masses involved in a decay, but identifying the endpoint of the visible mass distribution of the final states in a multibody decay mode, might let us calculate the mass difference between the last parent SUSY particle and the LSP. If we are looking at the right channels, we might be able to fit some of the parameters in the model using that kind of approach. In the cases where the NLSP to LSP decay is a two-body decay[1], we get a peak in the invariant mass plot. By counting events in these peaks, we can estimate the ratio of the cross sections of different final state modes, which also puts constraints on some of the model parameters.

Because the signals to be studied are produced in strong interactions (gluinos and squarks “feel” the strong nuclear force), the signal to background ratio is in general good. The SM background is dominated by QCD events, but SUSY itself is the largest contribution to the background (see figure 8.1). For that reason it is necessary to generate the whole SUSY cross section, not just a few specific channels.

One of the most popular starting point for studies of exclusive SUGRA signatures is the decay of the second lightest neutralino ($\tilde{\chi}_2^0$) into the LSP and either b-jets or lepton pairs (via the light Higgs boson or the neutral vector boson, if two-body decays are allowed by kinematics).

In chapters 6 and 7 a typical method of analysing supersymmetric channels will be established.

The purpose of constructing such analyses is threefold:

1. To verify that the proper software tools for this kind of analysis are available and operational. Descriptions of these tools are given in the next chapter.

1. An n-body decay will mean that n resonant (on-shell) states are produced, not n final state particles measured. Decays through virtual particles are thus separated from decays through real particles.

2. To generate a set of data, based on either SUGRA or GMSB, which might tell us something about how we should expect to detect and measure supersymmetric particles in ATLAS.
3. To validate detector design and performance by benchmark analyses.

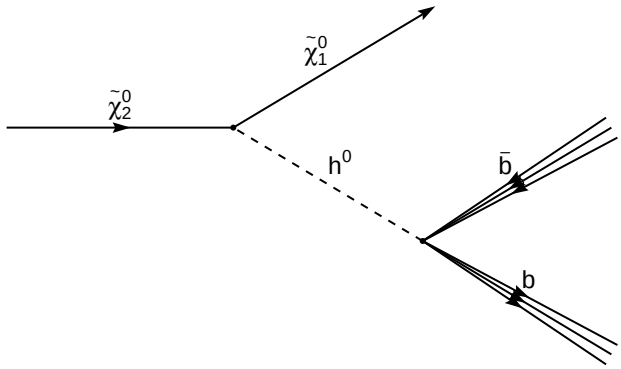

Figure 4.1a: Decay of the second neutralino into the light Higgs boson and the LSP.

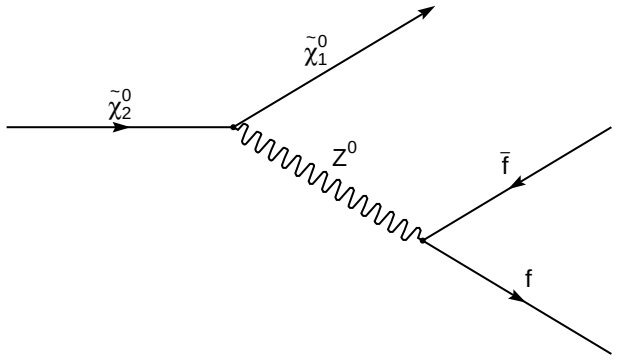

Figure 4.1b: Decay of the second neutralino into Z^0 and the LSP.

Six points in the SUGRA parameter space and four points in the GMSB parameter space have been put through this analysis, to make the results more general and wide covering. It is especially important to include examples of parameter points at which two-body decays of the second neutralino are allowed, as well as points at which only multi-body decays are allowed. That is due to the significant topological differences in the corresponding invariant mass plots.

In short terms, the analysis of a channel can be summarised as the following: Firstly, one defines which supersymmetric model is to be assumed, its parameter values, number of events to be generated, centre of mass energy, types of processes to be

included, limits on momenta etc. in a datacard file. Then one runs the main program (ISAGENE) that calls a Monte Carlo event generator (ISAJET, see 5.1.1) and a detector fast simulator (ATLFAST, see 5.2) as subroutines (figure 4.2). ISAJET is responsible for the calculation of what to come out of every event. ATLFAST is responsible for the simulation of how the ATLAS detector will interpret the signals delivered by ISAJET, and for sorting the resulting data into ntuples and even histograms. This is where PAW takes over, allowing us to plot data from the ntuples and histograms in a variety of ways.

In general, supersymmetric events will be very rare compared to SM events. For that reason it is common to impose several cuts upon the ntuples, so that events that are obviously pure SM will be ignored in the plot. By more thorough investigations of the phenomenology of the theory to be studied, one is able to specify the cuts to a higher precision, leaving as much interesting (in this context) physics as possible, while most of the background will hopefully vanish. A complete signal isolation is practically impossible, so a give-and-take compromise must be made.

In practice, the implementation of cuts requires a bit of programming to make the calculations upon the ntuple data. PAW allows us to call FORTRAN routines directly in the command prompt.

After adding cut by cut to the plots, one might find that the usage of kumac files greatly simplifies it all. Calling kumac files in PAW simply lets PAW execute the commands listed in the kumac file, line for line. It is also possible to define macros in the kumac files, so that one avoids making a new kumac file for each task. It is far easier to define a mask for each cut, and make kumac files to generate and open the masks in PAW. Then the calculations of the cuts are only made once for each ntuple.

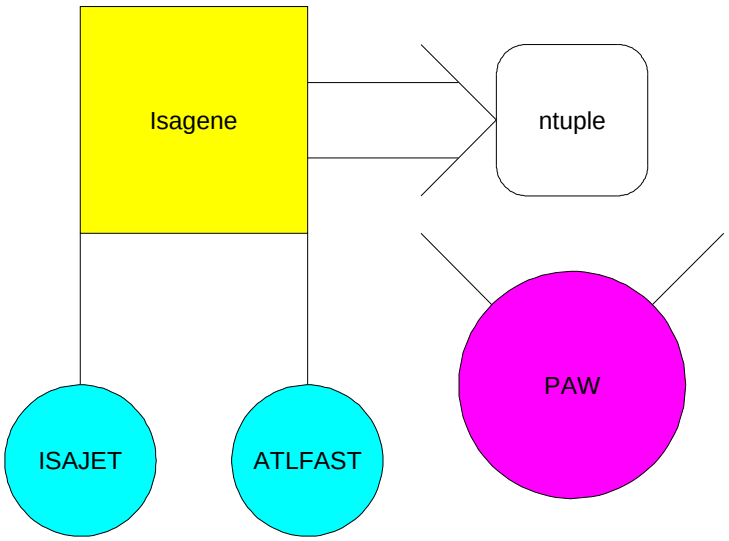

Figure 4.2: Schematic illustration of how the different software tools relate to each other.

5.0 Generators and Software Packages

When doing physics analysis the choice of software is always crucial for the quality of the results. In many cases one applies computer programs which are specifically designed for just a small number of processes, or maybe just one experiment (like ATLFAST). Other programs (such as PAW) are applicable to an extremely large number of different kinds of problems within high energy physics. The following subchapters contain some descriptions of the programs that have been used in the work with this thesis, and Monte Carlo methods in general.

5.1 Monte Carlo Event Generators

An event generator is a program which, given parameters provided by the user, calculates and delivers the contents in a set of physical events (in the context of the theory the user wishes to explore) to a program that handles the next step in the total analysis. In the case of this thesis; the fast detector simulator ATLFAST 2.0.

In any proper quantum theory, there is an element of statistic probability. That means that when one wishes to calculate an event, one cannot simply make a one-to-one calculation. Instead, one has to let a computer pick a quasirandom number generated from an initial seed. Ideally, the algoritm that generates the random numbers from the seed should have a large period (often up to 10^{43}). That is to make all numbers equally weighted in the constructed statistical distribution. This principal of systematic use of random sampling, as well as techniques for evaluating difficult integrals, is what characterises Monte Carlo methods.

To illustrate how a random sample can determine what physical process will end up in an event, consider the perhaps simplest case, where a system ‘A’ only has two equally probable final states ‘B’ and ‘C’. By picking a random number between zero and one, one can just decide that if the number is within the interval [0.0, 0.5), ‘B’ will be the final state. Otherwise, if the number is within the interval (0.5, 1.0], the system ends up in ‘C’.

Most practical situations are much more complicated than the one above. For instance in quantum field theoretical calculations, we often have to deal with some density probability function f (e.g. a matrix element in phase space) that is to be integrated over a finite, but multidimensional volume V. One is perhaps not able to calculate the integral analytically, but one is able to determine whether any given point is situated within the volume over which the integral is evaluated or not. That makes it possible to estimate the value of the integral by exploring the volume by N random samplings. According to the basic theorem of Monte Carlo integration [2], we then have:

$$\int_V f\,dV \approx V\langle f\rangle \pm V\sqrt{\frac{\langle f^2\rangle - \langle f\rangle^2}{N}} \qquad (5.0a)$$

(The error term after plus/minus does not have to be a Gaussian, so this should be considered an approximation.)

$$\langle f \rangle \equiv \frac{1}{N} \sum_{i=1}^{N} f(x_i) \tag{5.0b}$$

$$\langle f^2 \rangle \equiv \frac{1}{N} \sum_{i=1}^{N} f^2(x_i) \tag{5.0c}$$

One of the biggest disadvantages of this kind of method (which is sometimes called “hit-and-miss Monte Carlo”) is slow convergence. That means the variance of the results is large. Sometimes it is also hard to estimate the variance [10].

5.1.1 ISAJET 7.44

ISAJET is a Monte Carlo event generator for pp-, $p\bar{p}$- and e^+e^--reactions, where all calculations are made at parton level. It delivers hadronic final states to the detector simulator, based upon whatever underlying theory one wishes to investigate. Fundamental strong interactions are calculated in perturbative QCD. Parton and beam jet fragmentation is handled by a phenomenological model.

The event generation process is as follows [6]:

- The primary QCD hard scattering cross section is calculated according to the general formula $\sigma = \sigma_0 F(x_1, Q^2) F(x_2, Q^2)$, where σ_0 is a two-body cross section calculated by perturbative QCD, F a structure function, x_i momentum fraction and Q^2 the momentum transfer.
- Initial and final state QCD radiative corrections are added.
- Parton fragmentation into hadrons is conducted.
- Particles with τ_0 less than about 10^{-12} s are decayed.
- The remaining energy is used to produce minimum bias beam jets.

ISAJET also provides a decay table that contains information about the particles generated (type of particles, codenames of parent and/or daughter particles, cumulative branching ratios, types of decays etc.).

5.2 ATLFAST 2.0

ATLFAST is a fast detector simulation and physics analysis program for the ATLAS detector. The version used here is written in FORTRAN77, although an object oriented version is released. It includes jet reconstruction in the calorimeters, momentum/energy smearing for leptons and photons, magnetic field effects and missing transverse energy calculations [7]. The program can optionally provide a list of reconstructed

charged tracks. All detector dependent parameters are tuned to values given by the full simulations of the detector performance.

The level of simulation is somewhere between parton-level and full simulation. It is as accurate as the full simulation at mass resolution, jet reconstruction efficiency and missing transverse energy resolution, while it is not so accurate at reproducing efficiencies for lepton and photon isolation. The detector effects are simplified in ATLFAST compared to full simulations. It leaves out all effects due to details in the shapes of particle showers in the calorimeters and charged track multiplicity in jets. The parameterisation of photon, electron and muon momentum resolution, the hadronic calorimeter energy resolution and the effect of the ATLAS magnetic field on jet reconstruction are reasonably accurate.

Jet- and τ-tagging efficiencies and the inefficiency of mistagging jets were not included in the original version, but is now implemented in the supplementary package ATLFAST-B.

The primary purpose of ATLFAST is simulation and analysis of fully generated events, with selection of leptons and photons, jet reconstruction and labelling, and missing E_T estimations.

5.3 PAW

Physics **A**nalysis **W**orkstation is a multipurpose analysis package, developed at CERN in the mid eighties [13]. It is a visualisation program for scientific data analysis and presentation, conceived with high energy physics researchers in mind. The package consists of many different software tools, allowing the user to handle objects like ntuples, histograms, vectors etc. PAW may also be used for exploration of mathematical functions.

The main components of the package are as follows:

- KUIP (**K**it for a **U**ser **I**nterface **P**ackage) is the user/program dialogue handler.
- HBOOK and HPLOT are FORTRAN subroutine libraries that handle ntuples, histograms etc. (HPLOT is the graphics interface of HBOOK).
- HIGZ (**H**igh level **I**nterface to **G**raphics and **Z**ebra) is the interface between PAW and the graphics package on the local system.
- ZEBRA is a data structure management system that allows for creation and modification of data structures at execution time (this cannot be done in a satisfactory way in FORTRAN itself). It manages any data structure, but specifically lists and trees.
- MINUIT is a tool for finding, and analysing the shape of, minima of multiparameter functions. It also handles statistical analyses of curve fitting (χ^2, log-likelihood functions, computations of best fit parameters, their uncertainties and correlations).
- COMIS is the name of the FORTRAN interpreter.
- SIGMA (**S**ystem for **I**nteractive **G**raphical **M**athematical **A**pplications) is a scientific computing programming language. It handles scalars and arrays with operators in resemblance to FORTRAN.

6.0 The SUGRA Analysis

There are 32 supersymmetric particles in the minimal SUGRA model. Their masses and mixings are completely determined by the first four of the parameters given below. When one wishes to calculate particle masses, cross sections and branching ratios at an energy scale below the GUT scale, one has to solve iteratively a set of 26 Renormalization Group Equations (RGEs). The precision of the results depends on how many iterations one uses.

The SUGRA parameters [6]:

- m_0: the common scalar mass
- $m_{1/2}$: the common gaugino mass
- A_0: the common (soft SUSY breaking) trilinear coupling of the Higgs boson to any two sfermions[1]
- $\tan\beta \equiv v_u / v_d$[2]: the ratio of the two Higgs vacuum expectation values at the electroweak scale
- $\mathrm{sgn}\,\mu = \pm 1$: the sign of the Higgsino mass term in the Lagrangian

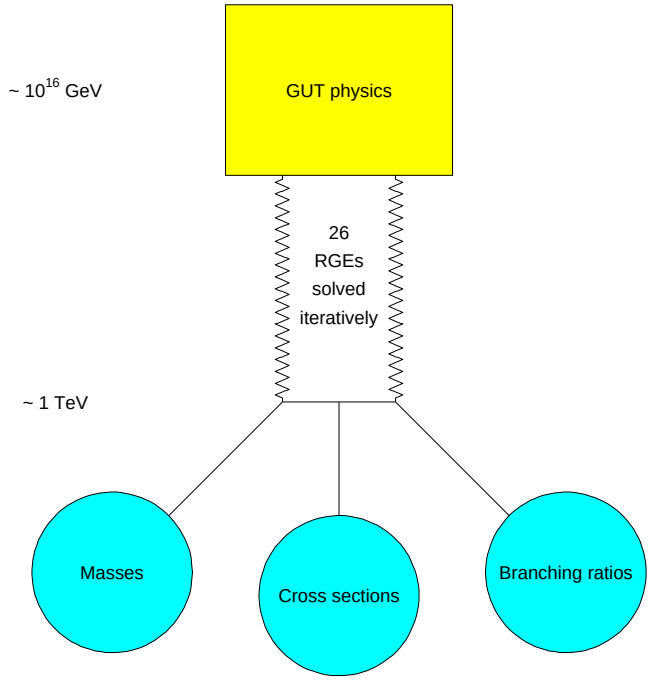

Figure 6.1: The RGE evolution from GUT to electroweak scale.

1. The first three parameters are at the GUT scale.
2. The ‘u’ and the ‘d’ are meant as an indication of the fact that the two Higgs fields are associated with mass generation of u- and d-type quarks and leptons separately.

The LHC Committee (LHCC) has chosen five official SUGRA parameter points (table 1) that possess certain features which make them interesting as starting points for an analysis. The reason none of the points have tanβ > 10 is because one has to include additional Yukawa couplings and mixing in the $\tilde{b}$ and $\tilde{\tau}$ sectors in such cases. That complicates the phenomenology. Point six was added by the ATLAS Collaboration as a sole example of such a point. The total SUSY production cross sections are quite different at the different points, mainly due to mass differences (table 2).

Table 3 shows MSSM particle masses (at tree level) at different SUGRA points (20.2.1 in [5]). First and second generation squarks and sleptons are degenerate in mass, so only first generation particles are listed. Loop corrections may have a significant impact on the MSSM masses. For instance, the lightest Higgs boson should have a mass of (120 ± 10) GeV [18] in any MSSM parameter constellation, loop corrections taken into account. That is probably one of the strongest predictions of the general MSSM scenario. The deviations from this value in table 3 are substantial.

As one might see, point two is the sole survivor (including the GMSB points) of the LEP2 Higgs search. The final runs of LEP2 have excluded the light Higgs boson mass up to 113.5 GeV with 95% confidence [20]. That does not mean that these parameter points are meaningless to study, because one can always tune up tanβ, so that the Higgsino content in the neutralinos is enlarged, making all the Higgs particles heavier.

There will be a more detailed discussion on each of the points in the following subchapters.

TABLE 1. The SUGRA points

Point	**m_0 (GeV)**	**$m_{1/2}$ (GeV)**	**A_0**	**tanβ**	**sgn μ**
1	400	400	0	2	+
2	400	400	0	10	+
3	200	100	0	2	-
4	800	200	0	10	+
5	100	300	300	2.1	+
6	200	200	0	45	-

TABLE 2. Total SUSY production cross sections (ISAJET 7.44)[a]

Point	1	2	3	4	5	6
σ (pb)	2.083	1.961	1515	25.00	16.67	102.7

a. Substantial deviations between the different versions of ISAJET are found.

TABLE 3. MSSM particle masses (GeV) at different SUGRA points [5]

Particle	Point 1	Point 2	Point 3	Point 4	Point 5	Point 6
$\tilde{g}$	1004	1009	298	582	767	540
$\tilde{\chi}_1^{\pm}$	325	321	96	147	232	152
$\tilde{\chi}_2^{\pm}$	764	537	272	315	518	307
$\tilde{\chi}_1^0$	168	168	45	80	122	81
$\tilde{\chi}_2^0$	326	321	97	148	233	152
$\tilde{\chi}_3^0$	750	519	257	290	497	286
$\tilde{\chi}_4^0$	766	538	273	315	521	304
$\tilde{u}_L$	957	963	317	918	687	511
$\tilde{u}_R$	925	933	313	910	664	498
$\tilde{d}_L$	959	966	323	921	690	517
$\tilde{d}_R$	921	939	314	910	662	498
$\tilde{t}_1$	643	710	264	594	489	365
$\tilde{t}_2$	924	933	329	805	717	517
$\tilde{b}_1$	854	871	278	774	633	390
$\tilde{b}_2$	922	930	314	903	663	480
$\tilde{e}_L$	490	491	216	814	239	250
$\tilde{e}_R$	430	431	207	805	157	219
$\tilde{\nu}_e$	486	485	207	810	230	237
$\tilde{\tau}_1$	430	425	206	797	157	132
$\tilde{\tau}_2$	490	491	216	811	239	259
$\tilde{\nu}_\tau$	486	483	207	806	230	218
h^0	95	116	69	112	93	112
H^0	1046	737	379	858	638	157
A^0	1044	737	371	859	634	157
$H^{\pm}$	1046	741	378	862	638	182

6.1 SUGRA Decay Signatures

Experimentally determining the SUGRA parameters seems to be an almost impossible task. However, studies of certain exclusive decay channels can at least put some constraints upon a few of the parameters. For instance, the ratio of $\sigma(\tilde{\chi}_2^0 \to \tilde{\chi}_1^0 h)$ to $\sigma(\tilde{\chi}_2^0 \to \tilde{\chi}_1^0 Z^0)$ is very sensitive to variations in tanβ and sgn μ. Analyses of these channels at point one and two (which only differ in tanβ) can therefore be a good place to start the determination of tanβ. That is exactly the starting point for this analysis. At point one the light Higgs mass is comparable to the mass of the Z^0 boson. That makes it hard to separate the two peaks in the corresponding b-jet invariant mass plot (which is customary to study in this kind of analysis). So it seems necessary to study the lepton decays of Z^0 as well. By counting dilepton events, we will know how many b-jet events that come from Z^0 decays (because the branching ratios of $Z^0 \to b\bar{b}$ and $Z^0 \to ll$ at tree level are known from precision electroweak studies).

The invariant mass of particles 1 through N is given by:

$$M(1, \ldots, N) = \sqrt{\left(\sum_{i=1}^{N} E_i\right)^2 - \left(\sum_{i=1}^{N} \vec{p}_i\right)^2} \tag{6.0}$$

where E_i and $\vec{p}_i$ denote the relativistic energy and momentum of particle number i.

Since the Higgs field couples to mass, the light Higgs boson (h^0) is most likely to decay either to b-jets, W or Z bosons. To remove b-jets that originate from top quarks (through other channels), one imposes a cut on the separation in the η–φ-plane of the two hardest (that is: highest transverse momenta) b-jets. Based on the assumption that b-jets that come from top quarks are more separated than those that come from Higgs decays, one keeps only events in which the two hardest b-jets have $\Delta R < 1.0$. The separation is given by:

$$\Delta R = \sqrt{(\Delta\eta)^2 + (\Delta\phi)^2} \tag{6.1}$$

Where Δη and Δφ denote the difference in (pseudo-) rapidity[1] and azimuthal angle (respectively) for the two jets. The latter entities are given by (6.2) and (6.3) [15].

$$\eta = -\log\left(\tan\frac{\theta}{2}\right) \tag{6.2a}$$

$$\tan\theta = p_T / p_z \tag{6.2b}$$

1. Often rapidity is used when one really means pseudorapidity. Pseudorapidity is an angular approximation to the rapidity, widely used in cases when we do not know masses and momenta.

where p_T is the transverse momentum and p_z is the longitudinal component of the momentum (along the beam axis). The azimuthal angle is the angle between the jets in the xy-plane (the z-axis is taken to be parallel to the beam direction). It is given by:

$$\cos\Delta\phi = \frac{\vec{p} \cdot \vec{p}'}{|\vec{p}| \cdot |\vec{p}'|} \tag{6.3}$$

where $\vec{p}$ and $\vec{p}'$ represent the momenta of the two jets in the transverse (xy-) plane.

Introducing the concept of pseudorapidity is a way of parameterising the momentum transfer in an event. Events with high momentum transfer are usually spread in large polar angles (θ), but most of the so called 'minimum bias' (inelastic) events have final states that are located closer to the beam axis. As seen from the formulae above, particles in the transverse plane (corresponding to a 90 degrees polar angle spread) will have pseudorapidity equal to zero, while particles along the beam axis will have an infinite value of pseudorapidity. In that way it is meaningful to impose cuts upon the events, requiring a low value of η to sort out only very inelastic events.

In subchapter 6.2 a standard analysis is constructed, customised for studying the signatures discussed above. This analysis is later on applied to other SUGRA points, and furthermore four points in the GMSB parameter space (chapter seven). The motivation for this is strong; we do not know what nature will present us, so we should be prepared to identify any signal that might appear in ATLAS.

6.2 SUGRA Points 1 and 2

These points have the highest masses of the SUGRA points, which is the main reason the total SUSY production cross section is the smallest among the points as well. As given in table one, these two parameter points only differ in the values of tanβ. This, and the fact that these points (together with point five) have substantial production of $\tilde{\chi}_2^0 \to \tilde{\chi}_1^0 h$ events, make these points attractive when one wishes to reconstruct the (invariant) mass resonance peak from the $h \to b\bar{b}$ channel.

At point one, tanβ is small. That means the lightest neutralinos are mainly gauginos and contain less Higgsinos. So the branching ratio for $\tilde{\chi}_2^0 \to \tilde{\chi}_1^0 h$ is almost 100%. The corresponding branching ratio at point two is just about 65%. That is because the Higgsino content in the neutralinos becomes larger when tanβ is increased to 10. The last 35% is almost only $\tilde{\chi}_2^0 \to \tilde{\chi}_1^0 Z^0$.

To isolate the relevant signal events, the following cuts were imposed upon the ntuples:

Dijet identification:

- More than 300 GeV missing energy in the transverse plane (see 3.6.5)

- At least two non-beauty jets harder than 100 GeV (most $\tilde{\chi}_2^0$s come from $\tilde{q}_L \to \tilde{\chi}_2^0 q$)
- Exactly two tagged b-jets harder than 100 GeV
- Separation (ΔR) of those two b-jets less than 1.0 (to reject $t \to bW^+$ and $\bar{t} \to \bar{b}W^-$ events)

Dilepton identification:

- More than 300 GeV missing transverse energy
- At least two non-beauty jets harder than 100 GeV
- One lepton pair (same flavour, opposite charge) harder than 10 GeV

Distributions of the entities mentioned in the cuts are given in figures 6.2 through 6.7. The total SUSY production cross section at point two is 1961 fb, according to ISAJET 7.44 calculations. The histograms correspond to 30 fb^{-1} of integrated luminosity, or 30% of a typical high luminosity LHC year. That corresponds to around 60 000 true SUSY events and ~ 10^{12} QCD background events; the cross section for two-jet QCD events - which is the totally dominant topology for the SM QCD background - is of order 10^7 larger than the total SUSY production cross section. A discussion of the background, and a justification of why only the SUSY background is represented in the plots in chapters 6 and 7 are given in chapter 8. Table 2 shows the total SUSY cross sections at the six SUGRA points.

The ntuple files become very big in cases where the SUSY mass scale is relatively low, so that the cross section grows big and the number of events corresponding to 30 fb^{-1} increases. In fact; only at SUGRA points one and two and GMSB points G1a and G1b the number of events generated in the analysis corresponds to an integrated luminosity of 30 fb^{-1}. In all the other cases, the values on the y-axis in the histograms are scaled up, corresponding to a 30 fb^{-1} ntuple.

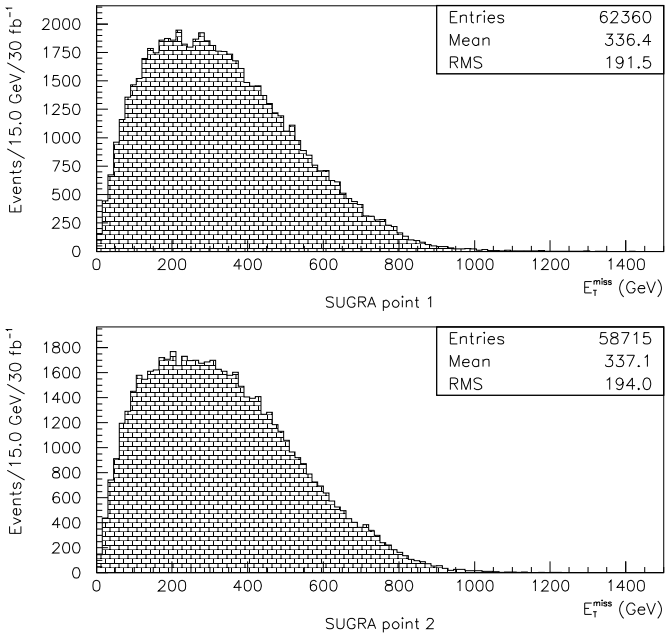

Figure 6.2: Missing transverse energy at SUGRA points 1 and 2.

About half of the events at both points contain missing energy greater than 300 GeV. This is a large fraction compared to other SUGRA and GMSB points, as we will see later, and the reason is that the LSP (which is the main source of the missing energy in the transverse plane) is in the final state of a relatively short decay chain. That means the lightest neutralino (the LSP) is able to carry away a larger momentum than it would at the end of a longer decay chain. A useful analogy to make this argument seem more reasonable, is to imagine a system of overlapping umbrellas in a waterfall. If the amount of water falling off an umbrella represents the momentum, we have that the more umbrellas (corresponds to a longer decay chain), the less water falling off each umbrella. So when the LSP production is dominated by a short decay chain, we will in general have more E_T^{miss}. The fact that the NLSP to LSP decay is a two-body decay also makes the phase space larger, thus allowing even harder LSPs in the final state.

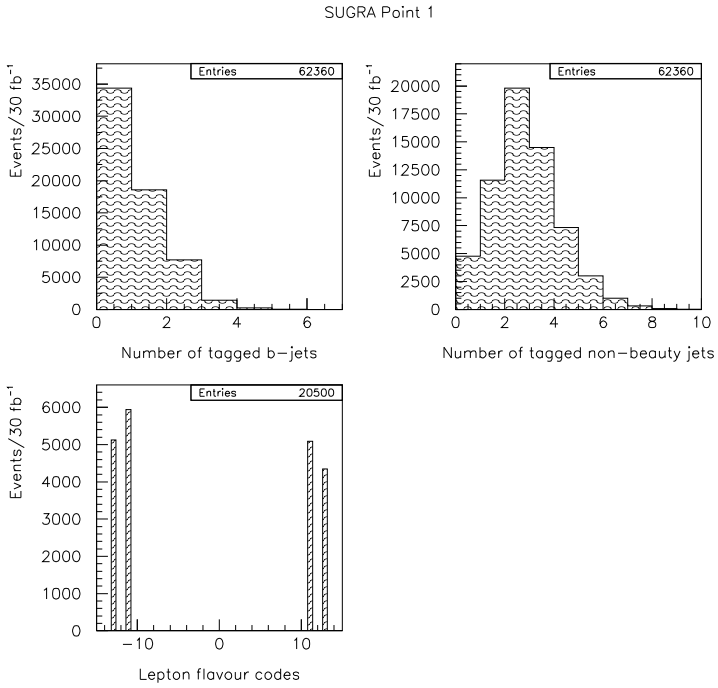

Figure 6.3: Flavour distributions at point one. The number of jets harder than 100 GeV. For the lepton flavour codes, 11 denotes electrons, 13 muons and negative numbers to their corresponding antiparticles.

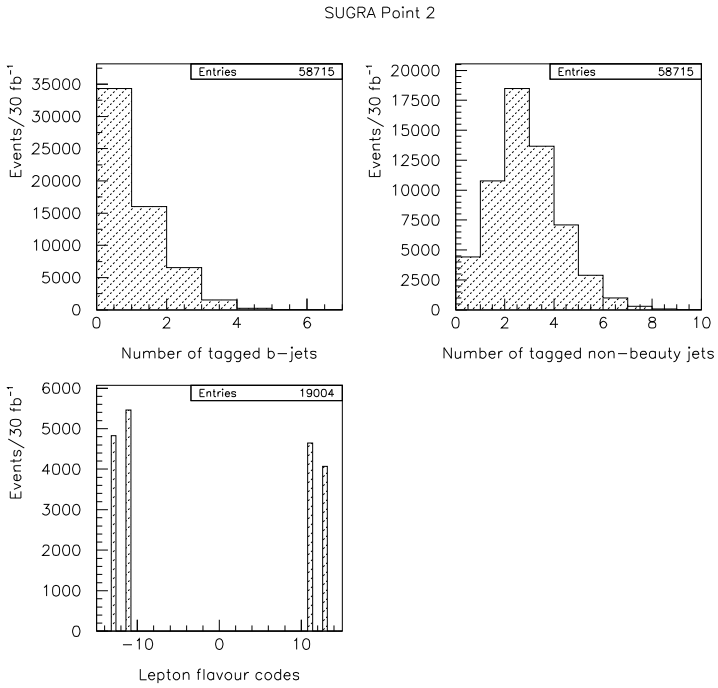

Figure 6.4: Flavour distributions at point two. The number of jets harder than 100 GeV. For the lepton flavour codes, 11 denotes electrons, 13 muons and negative numbers to their corresponding antiparticles.

At both points about 92% of the events contain at least one non-beauty jet harder than 100 GeV and approximately one third of the events contain at least one lepton in average. The number of tagged b-jets (p_T > 100 GeV) is somewhat larger at point one than at point two (45% and 42% of the events, respectively). This is because almost all neutralino decays (NLSP to LSP) at point one produce light Higgs bosons, which have a dominating branching ratio of decaying to two b-jets (because it couples to mass, and b-quarks are the heaviest particles kinematically available), while at point two, quite a few of the neutralino decays produce Z^0 particles, which is not dominated by b-jet decays in the same way.

There is no identification of τ leptons at any point in neither the SUGRA nor the GMSB analyses, because it decays so rapidly ($c\tau_0$ = 87.2 μm) into either electrons, muons or sometimes hadrons.

The excess of antimatter to matter in the lepton flavour distributions is due to the fact that the initial state particles are positively charged.

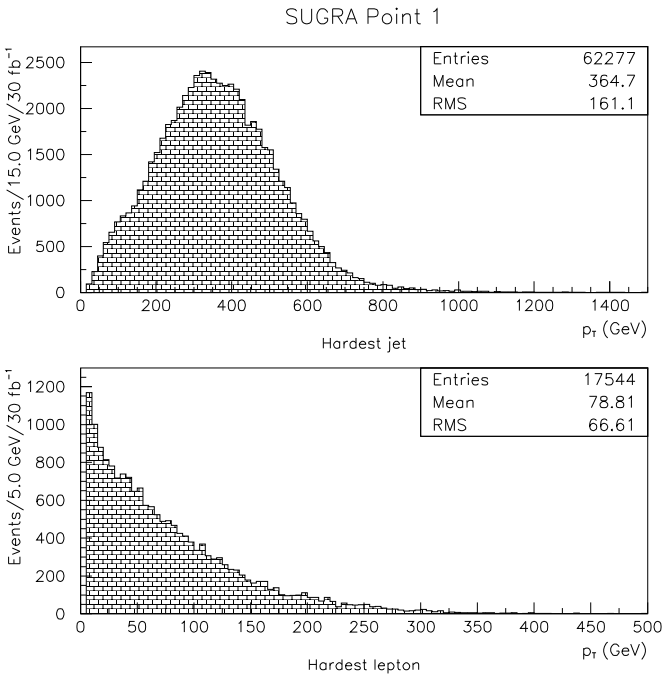

Figure 6.5: Transverse momentum distributions for the hardest jet/lepton in the event (point 1).

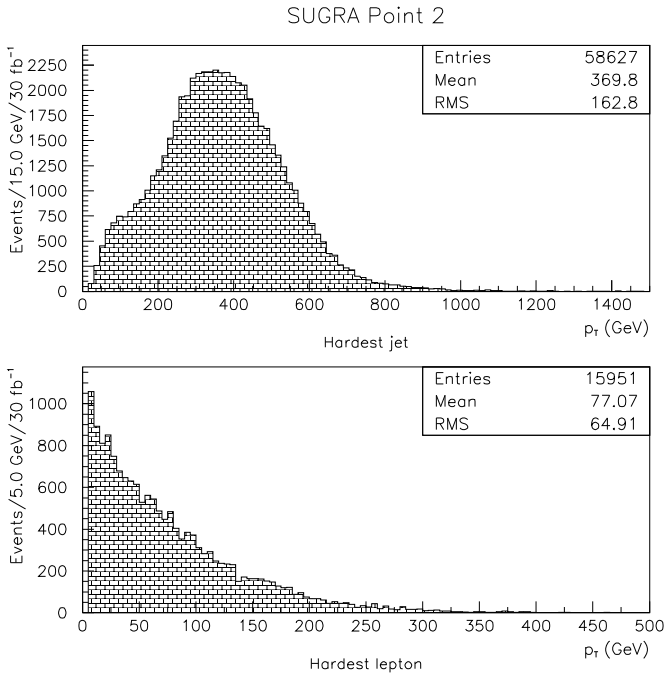

Figure 6.6: Transverse momentum distributions for the hardest jet/lepton in the event (point 2).

We see in figures 6.5 and 6.6 that point one and two have almost identical distributions of both jet and lepton transverse momenta. Furthermore, there is a large amount of events containing hard jets that will pass the cuts introduced in the beginning of this subchapter for b-jet and dilepton identification. The hardest jets and leptons are in general much harder at point one, two and five than at the rest of the SUGRA points. Taking a look at chapter 7, we see that also in the GMSB scenario we get many hard jets and leptons. In fact; only SUGRA points three, four and six have mean values of the hardest jet's p_T which are substantially below three times what is the limit in the cuts (100 GeV).

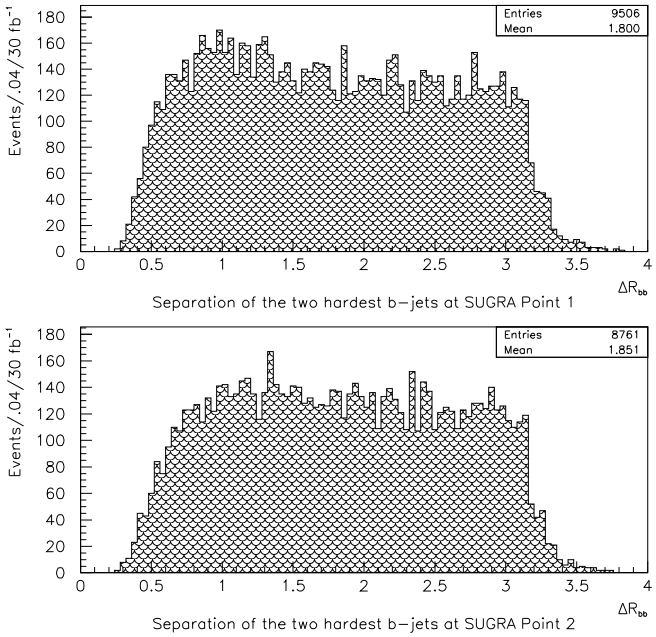

Figure 6.7: Separation of b-jets in the $\eta-\phi$-plane.

About 21% of the events in the upper histogram in figure 6.7 are below $\Delta R_{bb} = 1$, while about 18% pass the cut on separation in the lower histogram. Still, less than 10% of the events are left when the cut is imposed in the last histogram in both figure 6.8 and figure 6.10. That is probably because the cut on transverse momentum of the two hardest b-jets takes away about one fourth of the b-jet events alone. The combination of cuts will then be even stricter.

Figures 6.8, 6.9, 6.10 and 6.11 illustrate the effect of each cut on the invariant mass histograms:

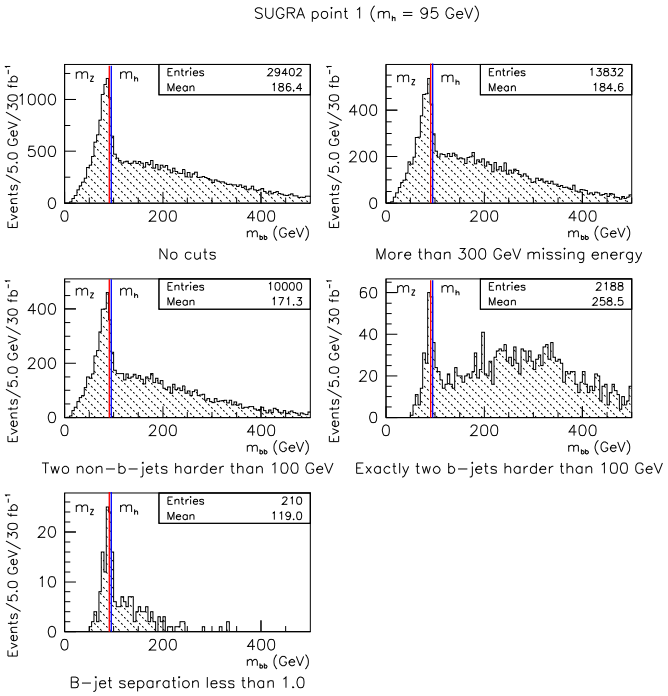

Figure 6.8: Invariant mass of b-jets at SUGRA point 1, cut by cut.

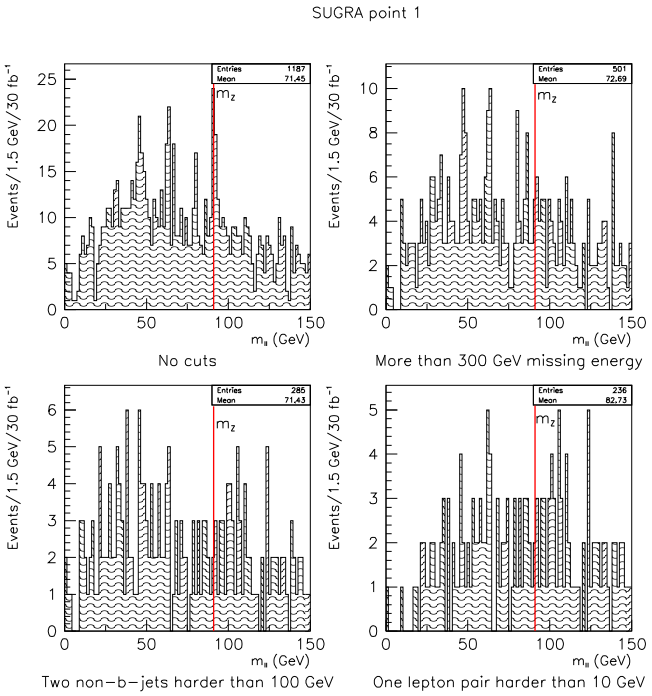

Figure 6.9: Invariant mass of lepton pairs at SUGRA point 1, cut by cut.

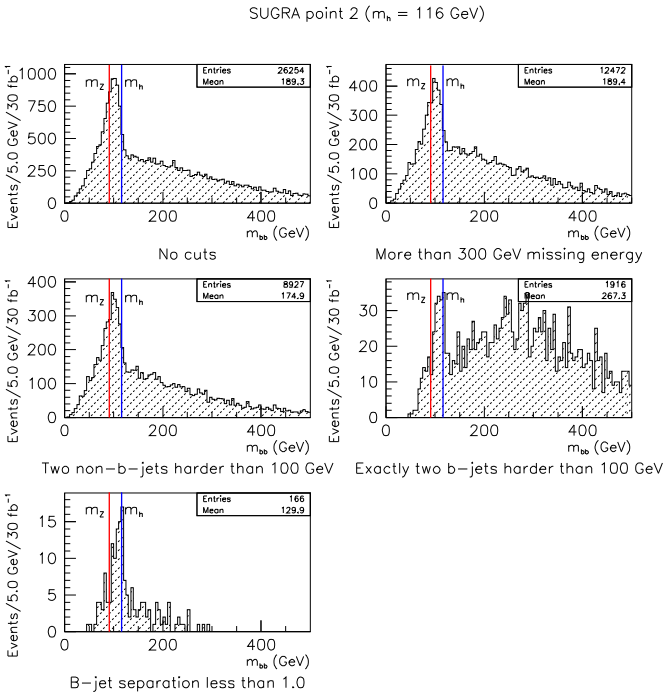

Figure 6.10: Invariant mass of b-jets at SUGRA point 2, cut by cut.

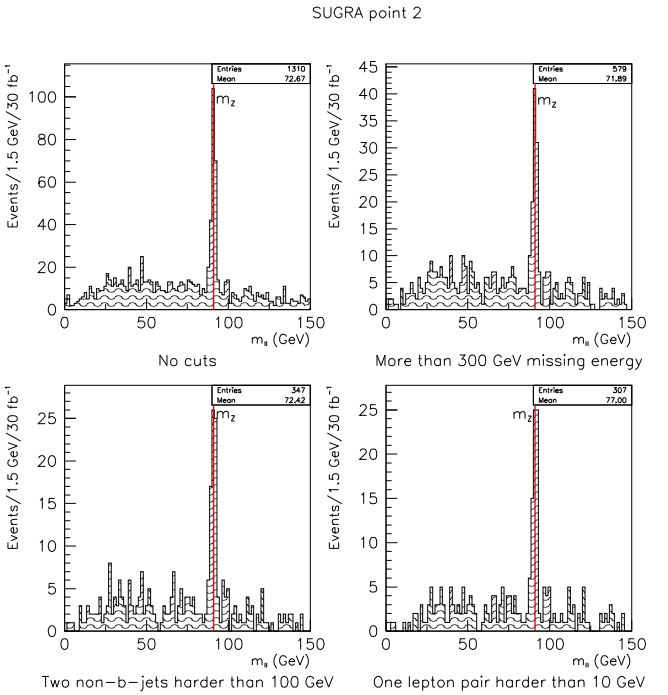

Figure 6.11: Invariant mass of lepton pairs at SUGRA point 2, cut by cut.

In figures 6.8 and 6.10 one can clearly see how the cut on separation reduces the background from b-jets originated from top quark decays.

The peaks in these histograms are much wider than the peaks in the dilepton signal histograms at point two. That is due to the energy smearing effect in the hadronic calorimeters, implemented in ATLFAST. The energy resolution is obviously much worse for hadrons than for leptons. The peaks in figure 6.10 are also somewhat wider than those in figure 6.8, which is due to the higher Higgs mass at point two. The peaks are quite asymmetrical, which is because of the shape of the background in that energy area.

The lacking sharp peak and the low number of events passing the cuts in figure 6.9 reflect the fact that the branching ratio for $\tilde{\chi}_2^0 \rightarrow \tilde{\chi}_1^0 Z^0$ is almost zero at point one.

6.3 SUGRA Point 3

Point 3 is a so called comparison point. That is because it gives a mass scale of about 300 GeV and a total SUSY cross section of roughly one nanobarn, so that existing accelerators would have a chance of finding something. This point is the one that is in most trouble, taking into account the results from the last year of LEP2. Both the light Higgs boson, the lightest chargino and the two lightest neutralinos are experimentally wiped out. It does not suffice to increase tanβ in this case. One would have to increase the mass parameters m_0 and $m_{1/2}$ as well, making it a totally different point.

The SUSY production cross section is dominated by gluino pair production. Light charginos and neutralinos have no two-body decays. Consequently, no peaks in the invariant mass histograms are found. The analysis is nevertheless carried out, to see what it might tell us anyhow. The entities involved in the signal cuts are discussed below.

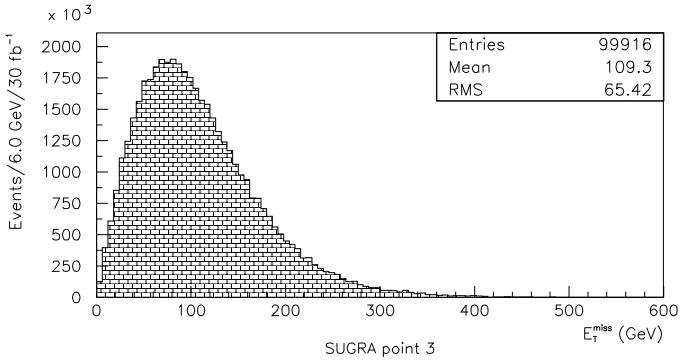

Figure 6.12: Missing transverse energy.

In this histogram we clearly see why the cut on missing energy is so high (it is often as low as 100 GeV in other SUGRA analyses). Only about 1% of the events will pass the cut on $E_T^{miss} > 300$ GeV. That is because the cross section is dominated by multibody decays and relatively long decay chains, so that the phase space of the LSP (the main

source of E_T^{miss}) is narrowed down. Consequently, hard LSPs are rare at this point. In that way, the cut lets us get rid of the events with b-jets and dileptons from other channels than those we are interested in. Most of the sparticles are also much lighter at point three than at any other SUGRA point, bringing the missing transverse energy values even lower.

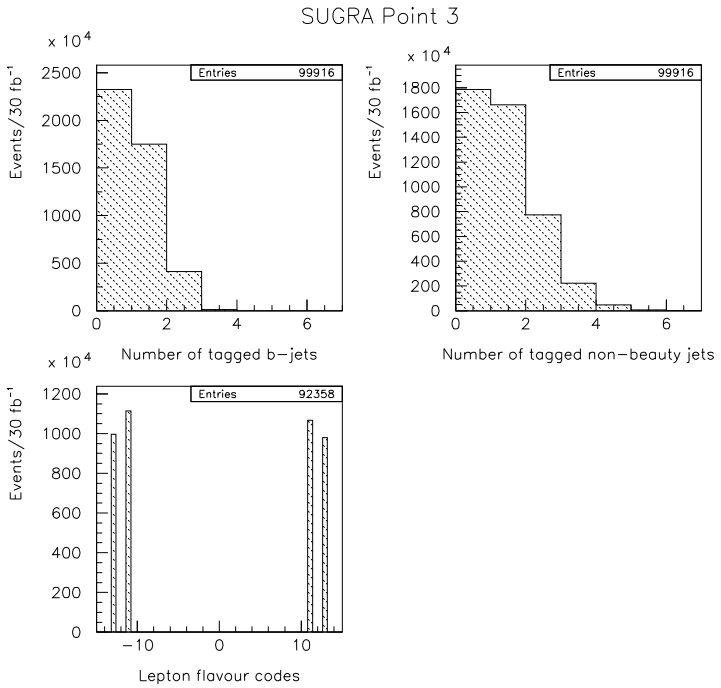

Figure 6.13: Flavour distributions at point 3. The number of jets harder than 100 GeV. For the lepton flavour codes, 11 denotes electrons, 13 denotes muons and negative numbers to their corresponding antiparticles.

As explained in subchapter 6.2, all the histograms in this subchapter are based on 100.000 events ntuples, scaled up to an equivalent integrated luminosity of 30 fb^{-1}. Among these 100.000 events there are 48 294 events with at least one tagged b-jet harder than 100 GeV, 60 253 events with at least one non-beauty jet harder than 100 GeV, 23 701 electrons, 24 741 positrons, 21 771 muons and 22 145 antimuons. Compared to points one and two, there are much fewer hard jets, while leptons are more common. That is because of the low mass difference of the two lightest neutralinos, suppressing hadron decays and leaving the mode $\tilde{\chi}_2^0 \rightarrow \tilde{\chi}_1^0 ll$ dominant.

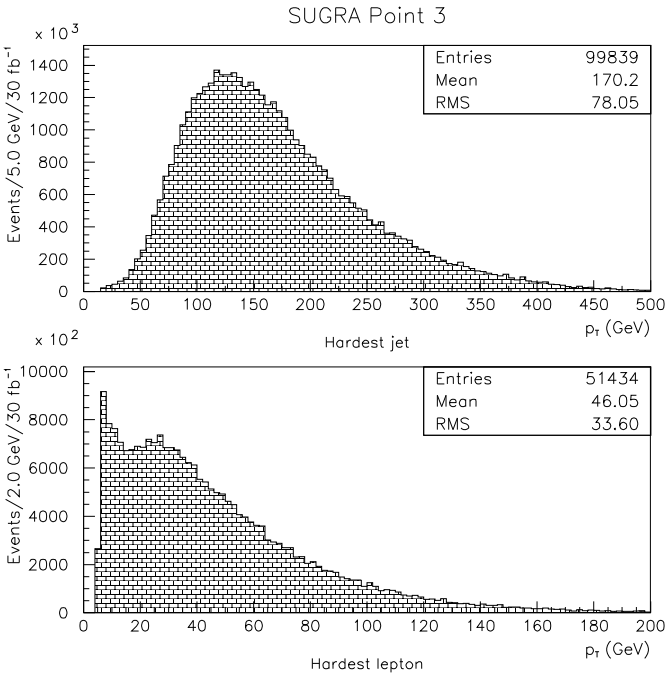

Figure 6.14: Transverse momentum distributions for the hardest jet/lepton in the event (point 3).

This is the point with the lowest mean value of the hardest jet's p_T and the second lowest mean value of the hardest lepton's p_T. Still, most of the events (82%) contain jets harder than 100 GeV, and almost half (47%) of the events have leptons harder than 10 GeV. That indicates that the cuts on transverse momenta are not very restrictive. As for the E_T^{miss} cut, those cuts are introduced to exclude jets and leptons from longer decay chains than the ones we are looking for (see 8.2 for more details). Especially from SM QCD cascade decays.

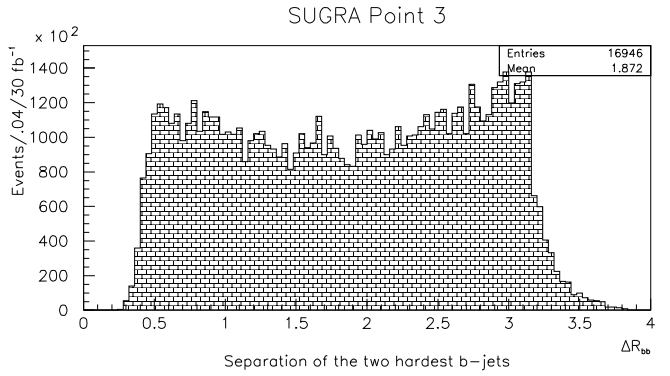

Figure 6.15: Separation of b-jets.

Approximately 22% of the events are below 1.0 in b-jet separation, which is more or less the same as for the other SUGRA points. It is in fact a little bit above, which might be due to the low mass scale, suppressing the production of the massive top quarks in squark and gluino cascade decays compared to SUGRA points with higher masses. B-jets that originate from top quark decays near the vertex are the ones we are seeking to sort out in the separation cut, because they are generally more separated in the η–ϕ-plane than the b-jets we are looking for.

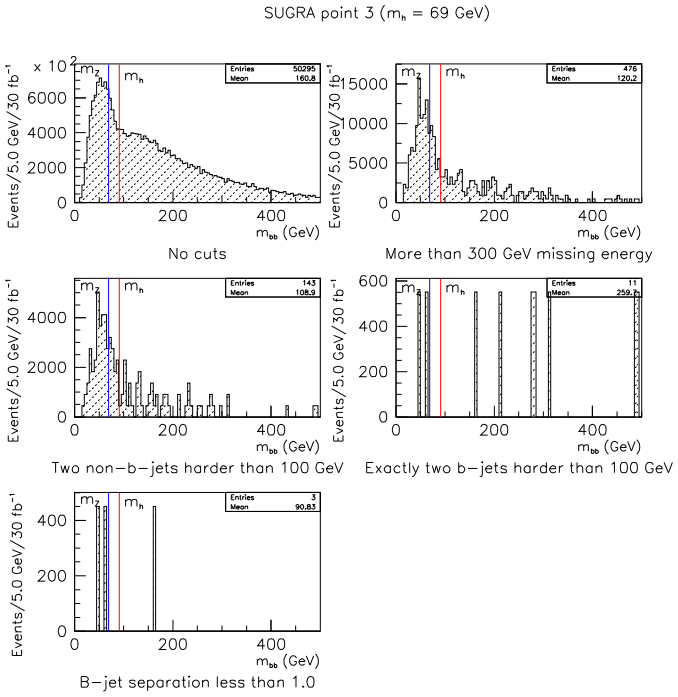

Figure 6.16: Invariant mass of b-jets, cut by cut.

The last histogram in figure 6.16 clearly shows the lack of b-jet production through neutralino to Higgs or Z^0 decay at this point (only three tagged b-jets pass all the cuts). Both b-jets and leptons come mainly from the channel $\tilde{g} \to \tilde{b}_1 b \to \tilde{\chi}_2^0 b\bar{b} \to \tilde{\chi}_1^0 llb\bar{b}$. Figure 6.17 shows that the dileptons from this channel are more likely to pass the signal cuts than the dijets.

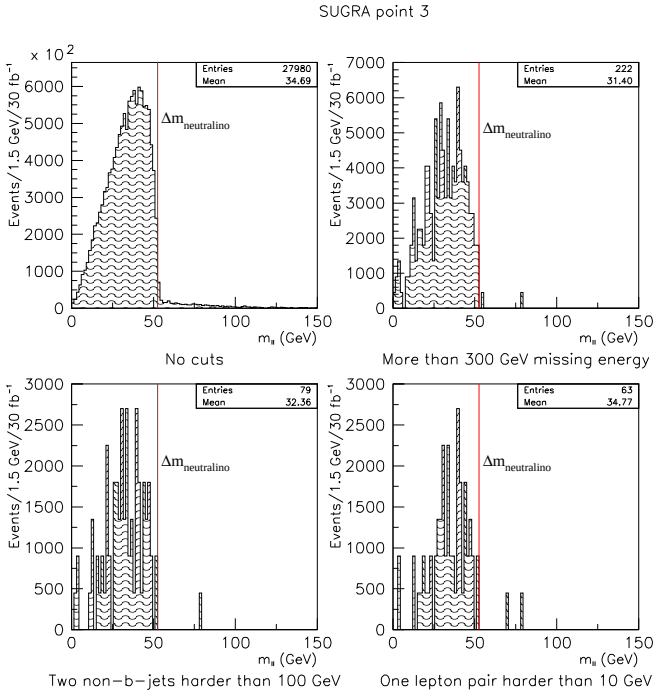

Figure 6.17: Invariant mass of lepton pairs, cut by cut.

The histograms above display no sharp peaks at approximately 91 GeV. That is expected, since all lepton pairs must originate directly from the neutralino decay. We do not have an intermediate real boson state as for point one and two.

It is also hard to identify any distinct endpoint in the lepton pair mass distribution after imposing the cuts, but it seems to be a bit above 50 GeV before the cuts. That corresponds well to the theoretical mass difference $\Delta m_{\tilde{\chi}_2^0, \tilde{\chi}_1^0} = 52.47$ GeV. The continous invariant mass distribution fits well to a three-body decay assumption, namely $\tilde{\chi}_2^0 \to \tilde{\chi}_1^0 ll$.

The signal is badly reduced by the cuts both for the dijets and for the dileptons (especially the dijets).

6.4 SUGRA Point 4

Point four is chosen to be close to the boundary beyond which electroweak symmetry breaking does not occur. This boundary depends on details in the implementation of the symmetry breaking, and is therefore not a sharp, model independent limit. Being close to this boundary means that μ is quite small, and the mixing between gauginos and Higgsinos is large. As for point three, light charginos and neutralinos have no two-body decays at point four. The point is suitable for gluino mass reconstruction, because gluino pair production dominates the SUSY cross section (the squarks are very heavy).

As for the previous subchapter, all the histograms here are based on 100.000 events ntuples, scaled to 30 fb^{-1}.

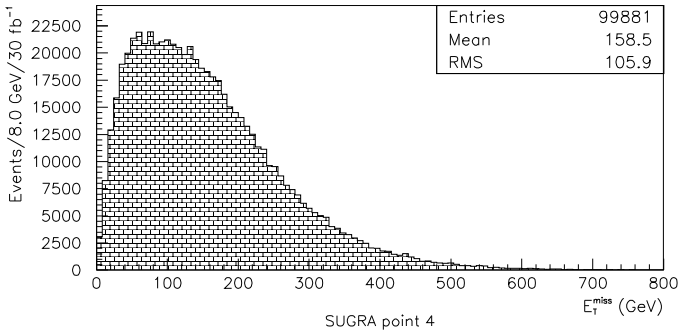

Figure 6.18: Missing transverse energy.

About 10% of the events are above $E_T^{miss} = 300$ GeV. That is second lowest of the SUGRA points. Only point three produces a smaller fraction of high missing energy events. The main reason for that is the lack of two-body decays, as for point three.

In the next figure, we see that 32% of all the events contain at least one tagged b-jet harder than 100 GeV, while 84% of the events have other flavour jets harder than 100 GeV. Both numbers are lower than at points one and two. The number of leptons is about the same.

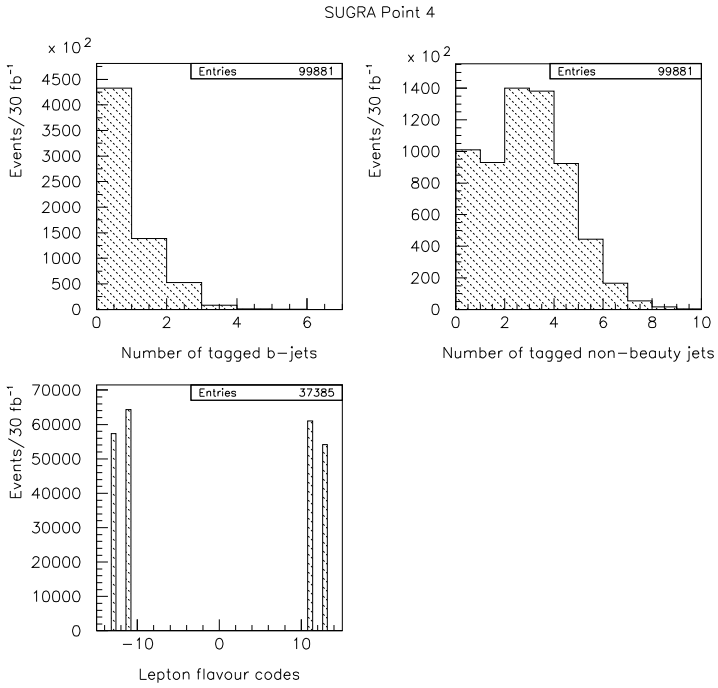

Figure 6.19: Flavour distributions at point 4. The number of jets harder than 100 GeV. For the lepton flavour codes, 11 and 13 denote electrons and muons (respectively) and negative numbers their corresponding antiparticles.

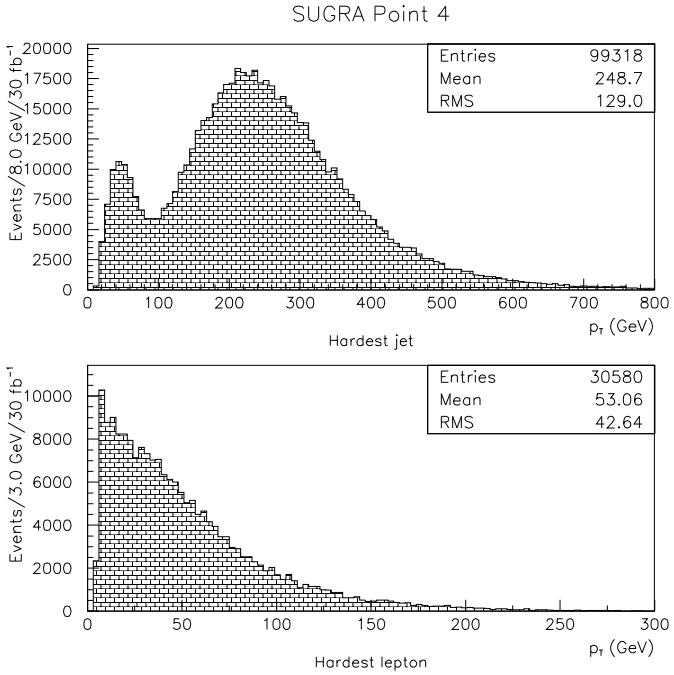

Figure 6.20: Transverse momentum distributions for the hardest jet/lepton in the event (point 4).

The shape of the upper histogram in figure 6.20 (hardest jet) is quite different to the other SUGRA points. One can see a small peak around 40 GeV, and then the usual broad peak, which is a bit higher than at point three, but still way below what was found at the first two points. This might mean there is a substantial production of jets with very narrow phase spaces, as well as jets from more open channels (as usual). The jets in the broad peak are most likely from gluino decays: $\tilde{g} \to q\bar{q}'\tilde{\chi}_1^{\pm}$ and $\tilde{g} \to q\bar{q}\tilde{\chi}_2^0$, where the prime on the antiquark means that if q is an up-type quark (u, c or t), $\bar{q}'$ is a down-type antiquark ($\bar{d}$, $\bar{s}$ or $\bar{b}$) or vice versa, making the total charge of the quark and the antiquark equal to ± 1.

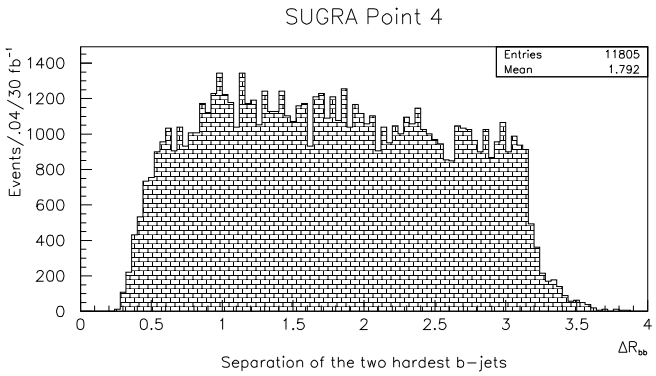

Figure 6.21: Separation of b-jets.

There are no big surprises in the histogram in figure 6.21; it looks pretty much like the ones in the other chapters, with a fraction of 21% of the events below 1.0.

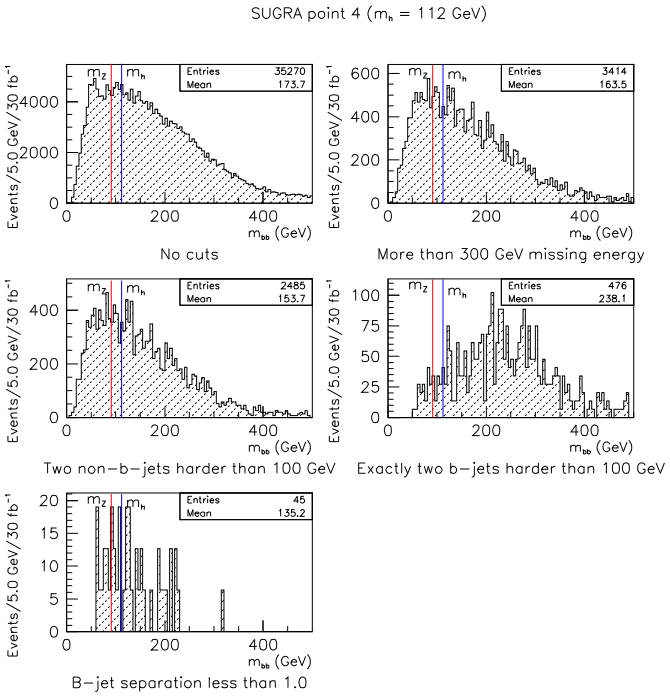

Figure 6.22: Invariant mass of b-jets, cut by cut.

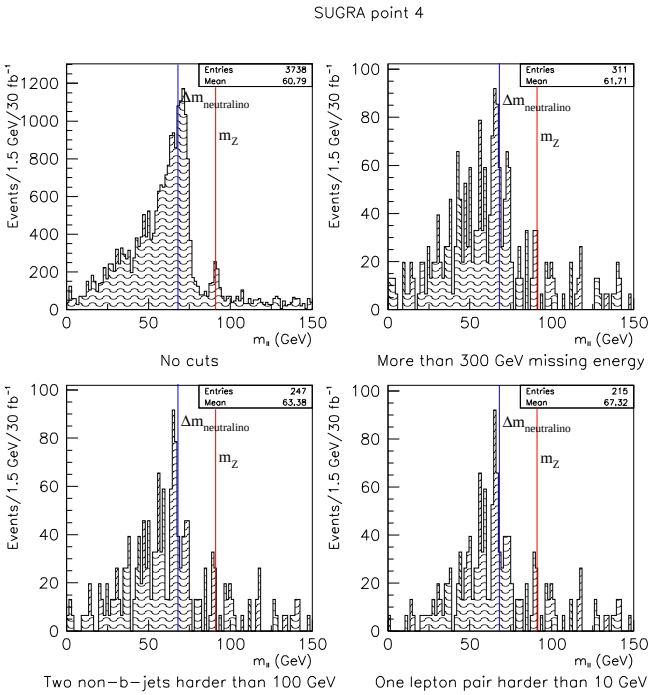

Figure 6.23: Invariant mass of dileptons, cut by cut.

Very few jets are left in the last histogram in figure 6.22 after all the cuts are imposed. There are no peaks around the light Higgs mass in any of the histograms, which is what

we expect, because the small μ at this point means the mixing between Higgsinos and gauginos in the neutralinos is strong. This in turn leads to a more gaugino-like coupling to light flavours (such as dileptons), rather than a Higgs-like coupling that would enhance Higgs production through neutralino decays. The few b-jets present are produced in Z^0 decays.

Also in the dilepton mass distribution we see that the cuts are not very suitable for this point. The signal from Z^0 decays is almost wiped out by the cuts. The small peak at the Z^0 mass is mainly from $\tilde{\chi}_2^{\pm} \rightarrow \tilde{\chi}_1^{\pm} Z^0$, but also $\tilde{\chi}_2^0 \rightarrow \tilde{\chi}_1^0 Z^0$, $\tilde{\chi}_3^0 \rightarrow \tilde{\chi}_{1,2}^0 Z^0$ and $\tilde{\chi}_4^0 \rightarrow \tilde{\chi}_{1,2}^0 Z^0$. The larger peak is at the mass difference $\Delta m_{\tilde{\chi}_2^0, \tilde{\chi}_1^0} = 68$ GeV from the channel $\tilde{\chi}_2^0 \rightarrow \tilde{\chi}_1^0 ll$, through a virtual Z^0 (conventionally denoted Z^*).

6.5 SUGRA Point 5

Point five is chosen to provide a good candidate for cold dark missing matter through the LSP. The LSP production corresponds to the universe having critical density $\Omega = 1$. This is the only SUGRA point with a non-zero value for A_0. Gluinos are heavier than the squarks at this point.

The channel $\tilde{\chi}_2^0 \rightarrow \tilde{\chi}_1^0 h$ is expected to be suitable as a starting point here in the same way as for point one and two.

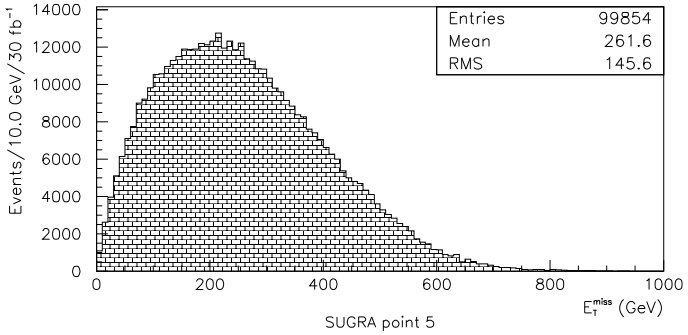

Figure 6.24: Missing transverse energy.

About 36% of the events are above 300 GeV, which is the highest fraction of all SUGRA and GMSB points except SUGRA points one and two. Hard LSPs from short decay chains in the final state is again the main reason for that.

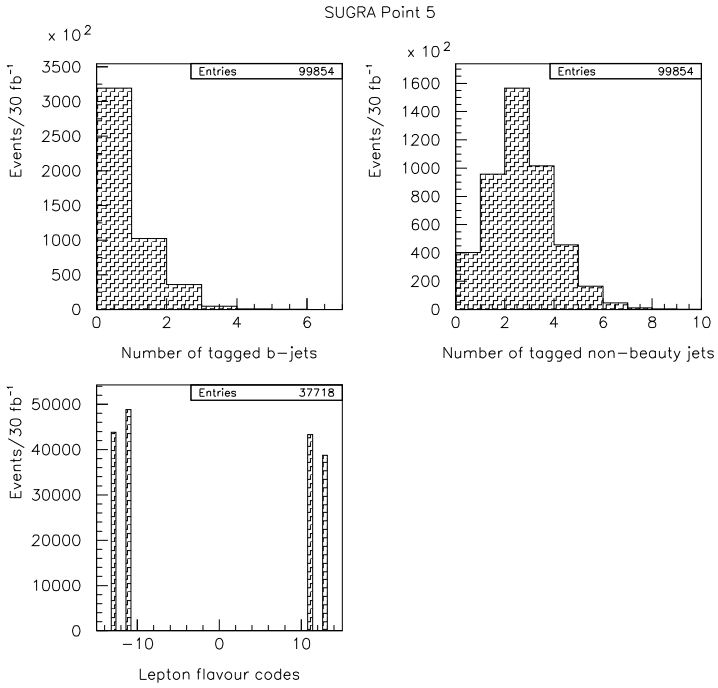

Figure 6.25: Flavour distributions at point 5. The number of jets harder than 100 GeV. For the lepton flavour codes, 11 and 13 denote electrons and muons (respectively) and negative numbers their corresponding antiparticles.

The number of leptons and hard non-beauty jets is roughly the same as for points one and two, which fits the assumption that the phenomenology is comparable. However, the number of hard tagged b-jets is somewhat smaller (31%, compared to 45% and 42%).

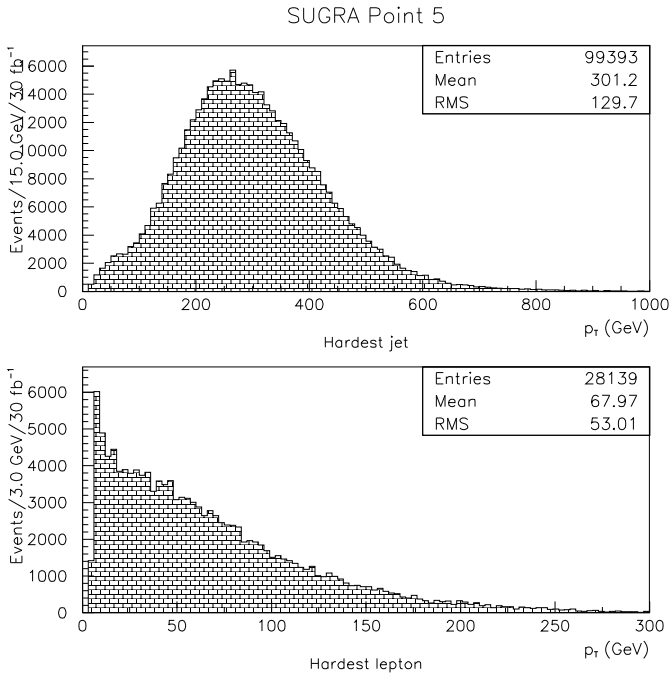

Figure 6.26: Transverse momentum distributions for the hardest jet/lepton in the event (point 5).

We see that there are numerous hard jet events. Most of the jets are from gluino and squark cascade decays, especially from $\tilde{q}_L \rightarrow \tilde{\chi}_2^0 q$ and $\tilde{q}_R \rightarrow \tilde{\chi}_1^0 q$.

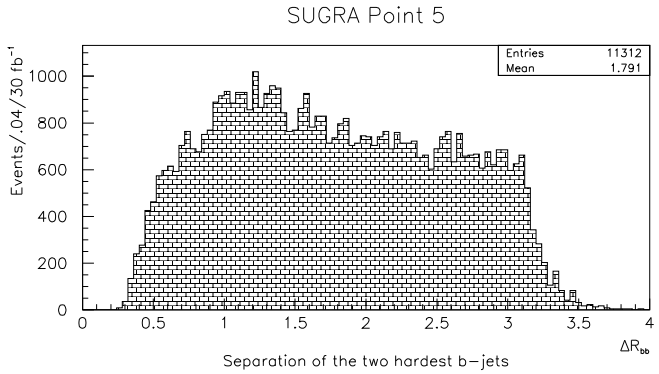

Figure 6.27: Separation of b-jets.

Only about 19% of the events are below the separation cut ($\Delta R_{bb} < 1.0$). This is not a substantial deviation from the other parameter points (points two and six actually have around 18%), but it is still quite low, and might be an indication on a rather large production of top-quarks through SUSY-channels (which is what we aim to exclude by the cut). In fact; the channels $\tilde{t}_1 \rightarrow \tilde{\chi}_i^0 t$ and $\tilde{b}_1 \rightarrow \tilde{\chi}_1^- t$ are significant at point five (the stop and the sbottom squarks are produced either directly or through gluino decays).

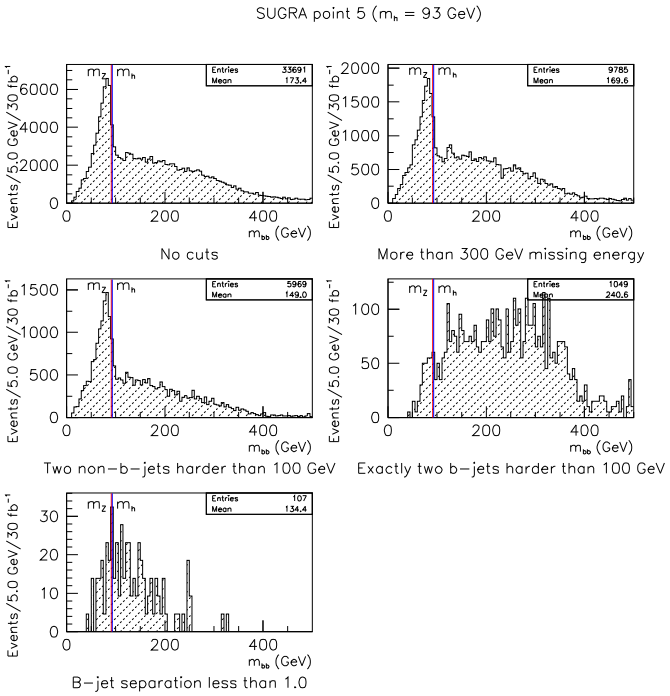

Figure 6.28: Invariant mass of b-jets, cut by cut.

Again we see how the cut on separation removes a great number of events from the second last to the last histogram, taking away top-quark contributions. A relatively sharp peak around the light Higgs mass and the mass of the Z^0 boson is found in the first three histograms, but is severely reduced by applying all the cuts.

The light masses of the right-handed sleptons open up the channel $\tilde{\chi}_2^0 \to \tilde{l}_R l \to \tilde{\chi}_1^0 ll$. That is the main source of the dilepton signal below. By experimentally identifying the endpoint of this distribution, one is able to estimate the mass difference of the two lightest neutralinos (nominally 111 GeV at this point).

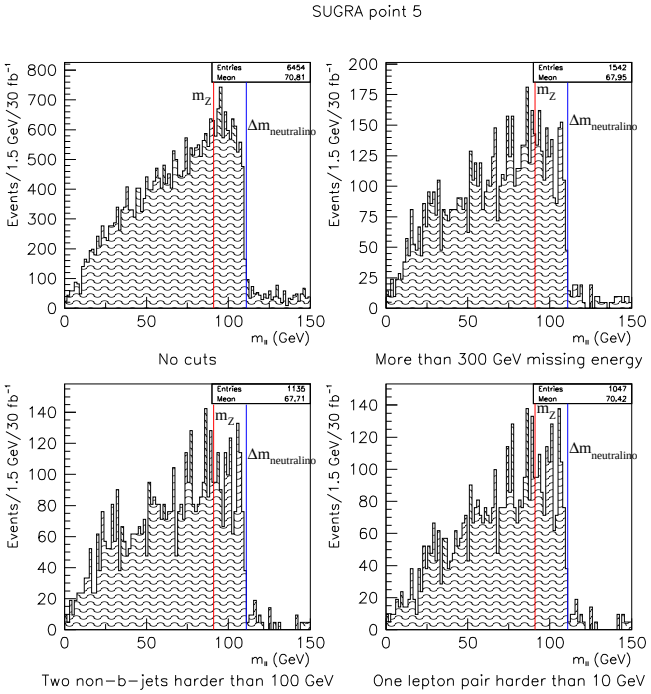

Figure 6.29: Invariant mass of lepton pairs, cut by cut.

6.6 SUGRA Point 6

This point is not one of the official LHCC SUGRA points, but was added by ATLAS as an example with a large value of tanβ. The splitting between $\tilde{\tau}_1$ and the other sleptons is increased with tanβ. The phenomenology is dominated by events containing τ's. That is because the masses are such that the usually dominating channels $\tilde{\chi}_2^0 \to \tilde{\chi}_1^0 h/Z^0$ and $\tilde{\chi}_2^0 \to \tilde{l}_{L,R} l$ (l and $\tilde{l}_{L,R}$ are first and second generation leptons and sleptons) are kinematically unavailable, making the modes $\tilde{\chi}_2^0 \to \tilde{\tau}\tau$ and $\tilde{\chi}_1^{\pm} \to \tilde{\tau}\nu_\tau$ totally dominant. The boson channels are forbidden because the neutralino masses are too light, while the slepton/lepton channels are forbidden because m_0 is too large. An analysis based upon hadronic τ decays will therefore be more reasonable than an analysis of the kind applied here.

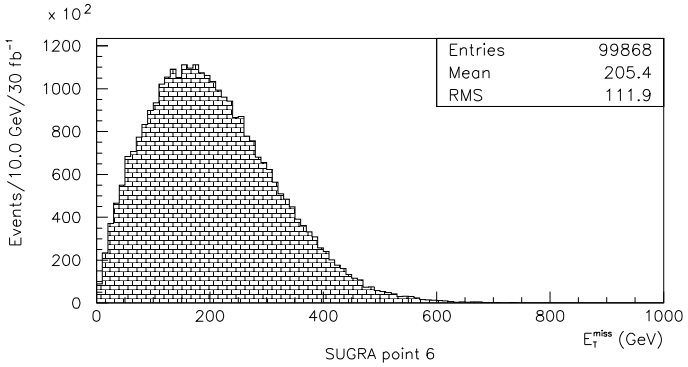

Figure 6.30: Missing transverse energy.

Around 20% of the events have missing energy above 300 GeV, which is a medium amount compared to the other points. A relatively larger part of the missing energy here is due to neutrinos, for reasons discussed in the beginning of this subchapter.

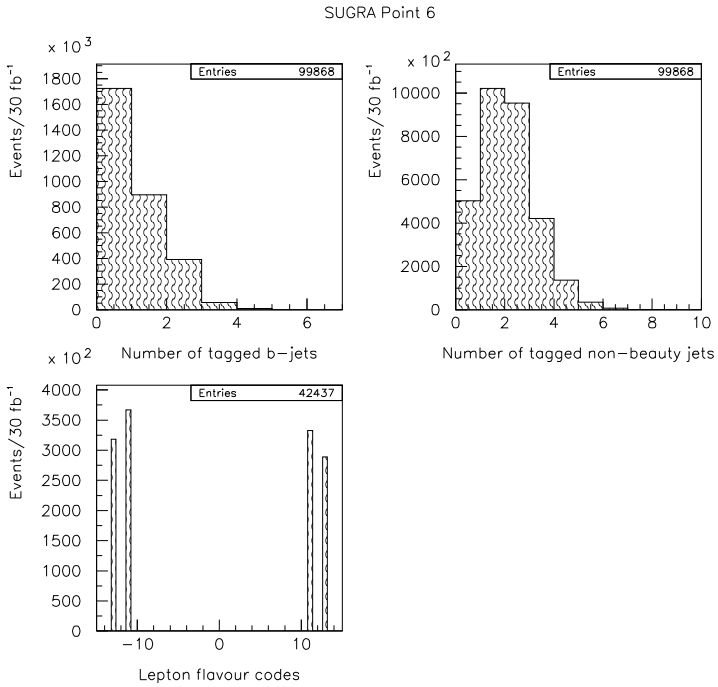

Figure 6.31: Flavour distributions at point 6. The number of jets harder than 100 GeV. For the lepton flavour codes, 11 and 13 denote electrons and muons (respectively) and negative numbers their corresponding antiparticles.

Apparently, there is a high production of hard jets (44% b-jet and 84% non-b-jet events) and leptons (42 437 leptons in 100 000 events) at this point, too.

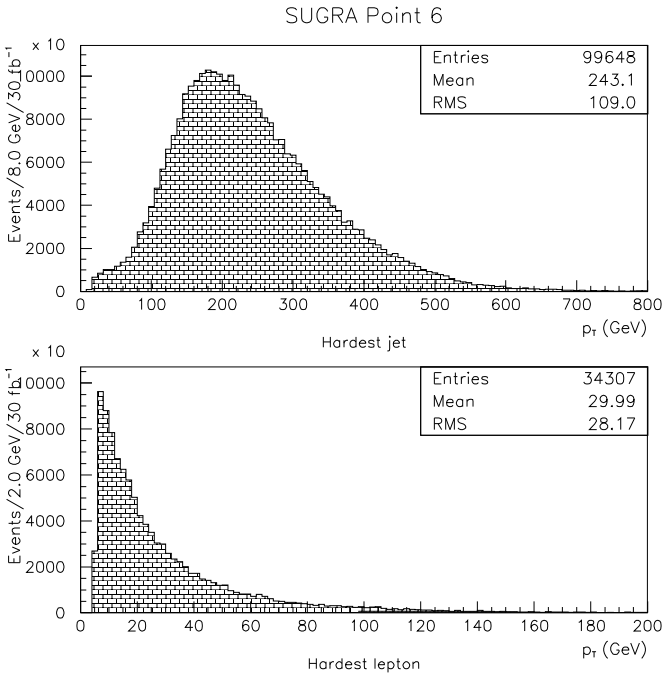

Figure 6.32: Transverse momentum distributions for the hardest jet/lepton in the event (point 6).

The shape of the jet p_T curve is similar to the one at point three, but the values are about 50-100 GeV above. The lepton p_T curve is very steep, and flattens out at a very low value. Only point three is lower.

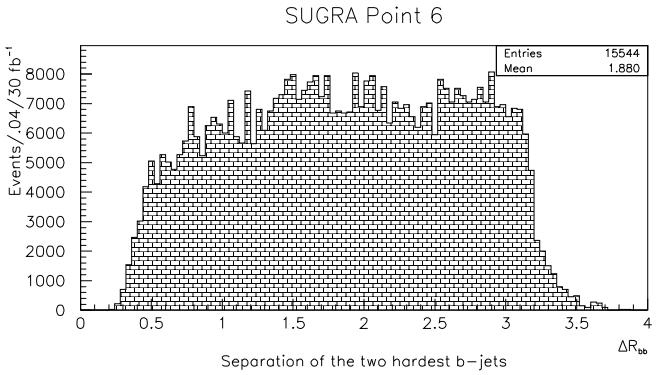

Figure 6.33: Separation of b-jets.

Roughly 18% is below 1.0 in this histogram. The main source of the top quarks responsible for such a low value is squark and quark production through gluino decays.

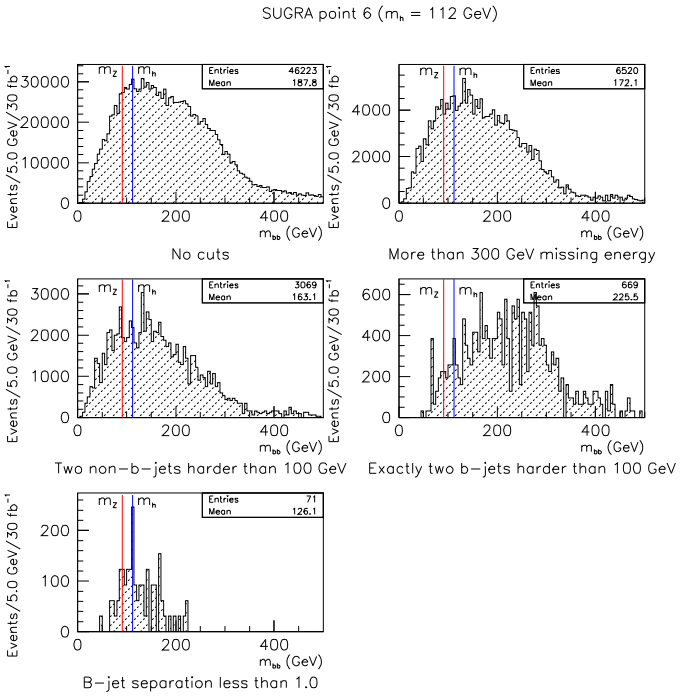

Figure 6.34: Invariant mass of b-jets, cut by cut.

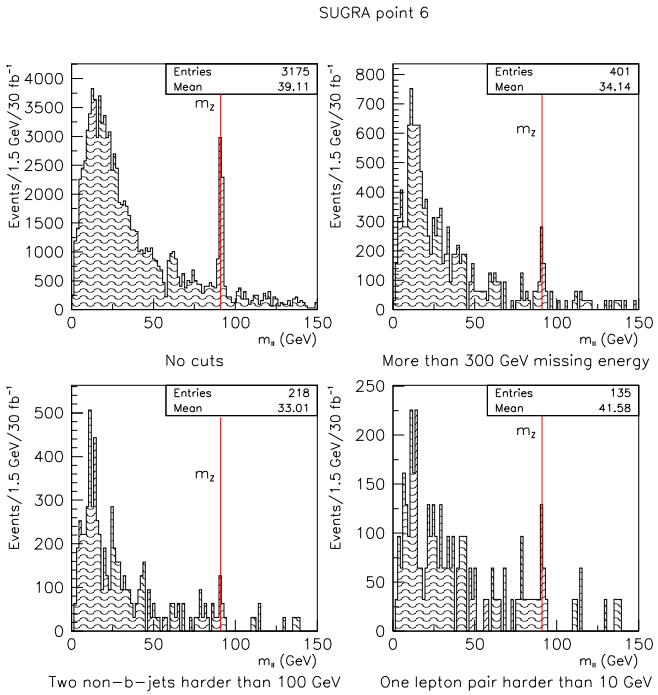

Figure 6.35: Invariant mass of dileptons, cut by cut.

This point is perhaps the least suitable of the six SUGRA points for this kind of analysis, because it does not allow any of the decay channels that have been discussed above.

The b-jets that are seen in figure 6.34 are from gluino decays (some from $\tilde{\chi}_3^0 \to \tilde{\chi}_2^0 Z^0, Z^0 \to b\bar{b}$), while the dileptons are mainly from $\tilde{\chi}_3^0 \to \tilde{\chi}_2^0 Z^0, Z^0 \to ll$ and various tau decays. Consequently, no resonance peaks or distinct endpoint three-body decay invariant mass distributions are seen.

6.7 Summary

Six parameter constellations, designed for a variety of physical quantities, have been put through exactly the same analysis. Invariant masses of b-jets and pairs of leptons have been reconstructed by isolating the signal by a set of cuts on kinematic variables as momentum and missing energy in the transverse plane of the detector, and separation in the plane that is spanned by the azimuthal angle ϕ and the pseudorapidity η.

The background from Standard Model physics was not included in the histograms, mainly because it is ignorable compared to the signal and to the background from SUSY physics, which is automatically included (the whole SUSY cross section is generated).

For most of the points, we were able to get something meaningful out of the dilepton invariant mass histograms, even if the channel for which the cuts were customised, was closed at certain points. The only major exception is point one, at which no interesting physics could be deduced from the mass histogram. At all the other points where the channel $\tilde{\chi}_2^0 \to \tilde{\chi}_1^0 Z^0 \to ll + E_T^{miss}$ was kinematically forbidden, it was possible to recognize other decay modes. And in cases where the dominant neutralino decay mode was a multibody decay, we were able to identify the endpoint in the mass distribution, thus making an estimate on the mass difference of the two neutralinos.

When doing the dijet invariant mass reconstruction, only points one, two and five gave us something meaningful. In other words: we did not get anything “for free” as for the dilepton analysis, where the cuts seemed to suit other channels as well as those we were looking for. It is thus tempting to state that the dilepton analysis covers a much wider part of the parameter space than the dijet analysis.

As for the various distributions of the entities involved in the isolation cuts, we learned that at points where the second lightest neutralino is allowed to decay via a slepton and a lepton, the transverse momenta in the final state are much lower on average than in the cases where the LSP is produced directly.

All in all, this chapter provided us with a qualitative analysis of some general aspects of the SUGRA phenomenology. A quantitative analysis for the fixing of parameter values and so on requires a much bigger effort, if the same parameter space coverage is wanted. More luminosity would also be necessary in most cases.

7.0 The GMSB Analysis

It seems natural to investigate what a competing model to SUGRA would provide if we do the exact same analysis upon it. Nature may perhaps allow both supergravity and gauge mediated SUSY breaking to occur, but in the case of only one source of SUSY breaking we should be somewhat prepared to find either of these two alternatives. Nature might of course provide something very different as well.

After applying a set of constraints upon the GMSB model, one ends up with the following parameters, from which 'everything' might be derived (through the RGE evolution, as in SUGRA models) [5]:

M_m: The messenger scale at which SUSY breaking is communicated from the hidden sector through $SU(3) \times SU(2) \times U(1)$ gauge interactions. This scale is assumed to be much lower than the Planck scale. Maybe even close to the electroweak scale.

$\Lambda \equiv F_m / M_m$, where F_m is the scale at which SUSY is broken in the separate sector. F_m is believed to be about $(10^{11}\ \text{GeV})^2$ in both the SUGRA and the GMSB models.

N_5: The number of messenger fields. Or in other terms: the number of equivalent vector-like representations of $SU(5)$. Such representations might be $\underset{\sim}{5} \oplus \underset{\sim}{\bar{5}}$ or $\underset{\sim}{10} \oplus \underset{\sim}{\overline{10}}$. The value of N_5 determines what particle is the next lightest supersymmetric particle (the NLSP); N_5 equal to one means that the NLSP is the lightest neutralino, while N_5 greater than one makes the NLSP a right handed slepton. The LSP is always the gravitino ($\tilde{G}$) in the GMSB scenario.

C_{grav}: The ratio of the gravitino mass to the value it would have if the only source of SUSY breaking is from the hidden messenger sector (based on the assumption that there might be other hidden, perhaps more complex, SUSY breaking sectors that can contribute to the gravitino mass).

Finally there are tanβ and sgn μ as in other MSSMs. The sign of μ is equal to +1 for all the points subjected to this analysis, and is therefore omitted in table 3.

Similar to the LHCC SUGRA points, there are four points in the minimal GMSB parameter space that are chosen for detailed studies. As seen in table 3, points G1a differ from G1b only in the value of C_{grav}. G2a differs from G2b in the same way.

TABLE 4. The GMSB points [5]

Point	**Λ (TeV)**	**M_m (TeV)**	**N_5**	**tanβ**	**C_{grav}**	**NLSP**
G1a	90	500	1	5.0	1.0	$\tilde{\chi}_1^0$
G1b	90	500	1	5.0	1000	$\tilde{\chi}_1^0$
G2a	30	250	3	5.0	1.0	$\tilde{\tau}_1$
G2b	30	250	3	5.0	5000	$\tilde{\tau}_1$

The phenomenology of the minimal GMSB model is quite different at different parameter points. At point G1b it is almost identical to that of SUGRA (qualitatively), but the total SUSY production cross section is slightly different (table 5). The particle masses relevant in this analysis are listed in table 7.

TABLE 5. Total SUSY production cross sections

Point	**G1a**	**G1b**	**G2a**	**G2b**
σ_{SUSY} (fb)	5495	5495	17 510	17 495

TABLE 6. Expected number of SUSY events after $\int L dt = 30$ fb^{-1}

Point	**G1a**	**G1b**	**G2a**	**G2b**
N_{SUSY}	164 850	164 850	525 300	524 843

TABLE 7. Relevant particle masses (GeV) [5]

	h^0	$\tilde{\chi}_1^0$	$\tilde{\chi}_2^0$	$\Delta m_{\tilde{\chi}_2^0, \tilde{\chi}_1^0}$
G1	110	119	224	105
G2	107	116	204	88

The standard analysis is carried out point by point in the two following subchapters. The points are treated as pairs because of the major phenomenological similarities (as reflected by the masses and cross sections in tables 4, 5 and 7).

7.1 GMSB Points G1a and G1b

The most important reason why point G1b is comparable in phenomenology to SUGRA, is that the NLSP has long enough lifetime to escape detection in ATLAS. It will therefore appear to be the LSP at the bottom of the decay chain. And the NLSP at GMSB points G1a and G1b is just the LSP from the SUGRA model, namely the lightest neutralino. Occasionally the neutralino will decay inside the tracker volume, giving rise to an isolated photon that does not point to the interaction vertex. Identification of such photons is considered an extremely important way of figuring out how SUSY is broken at the global scale, through the estimation of C_{grav} by measurements of the lifetime of the NLSP. $C_{grav} > 1$ would tell us that there is more than one source of SUSY breaking.

At both points all squarks are heavier than the gluinos. That represents an important difference from SUGRA points one, two and five (which are otherwise quite similar).

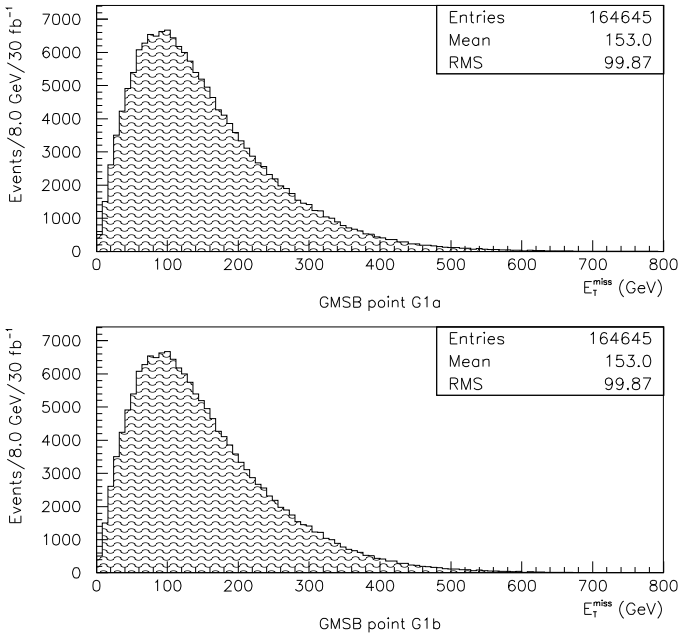

Figure 7.1: Missing transverse energy.

Only 9% is above the limit at 300 GeV at both points, which is the second lowest fraction of all SUGRA and GMSB points. SUGRA point three is the only one with a smaller fraction passing the E_T^{miss} cut (approximately 1%). SUGRA point four has about the same as G1a and G1b (10%). The low fraction here is no surprise, since the LSP (the gravitino) is always at the bottom of a long decay chain, for instance $\tilde{q}_L \to \tilde{\chi}_2^0 q, \tilde{\chi}_2^0 \to \tilde{l}l \to \tilde{\chi}_1^0 ll \to \tilde{G}ll\gamma$. There are five particles in the final state in this chain, while the chains considered in 6.2 had only four particles in the final state ($\tilde{q}_L \to \tilde{\chi}_2^0 q, \tilde{\chi}_2^0 \to \tilde{\chi}_1^0 h/Z^0 \to \tilde{\chi}_1^0 f\bar{f}$).

The first channel mentioned above is also an important source of the large number of leptons. There is almost one lepton per event in average, as seen in figures 7.2 and 7.3 below, while only about 23% of the events contain a b-jet harder than 100 GeV. That is lower than all the SUGRA points. 87% of the events have at least one non-beauty jet harder than 100 GeV, which is roughly the same as all GMSB and SUGRA points in consideration, except SUGRA point three (60%). G1a and G1b have very similar distributions of leptons and hard jets.

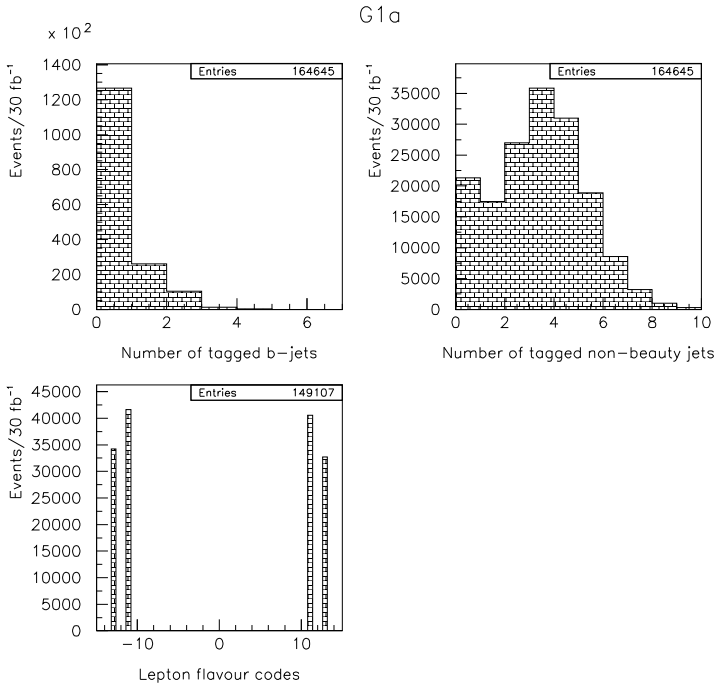

Figure 7.2: Flavour distributions at point G1a. The number of jets harder than 100 GeV. For the lepton flavour codes, 11 and 13 denote electrons and muons (respectively) and negative numbers their corresponding antiparticles.

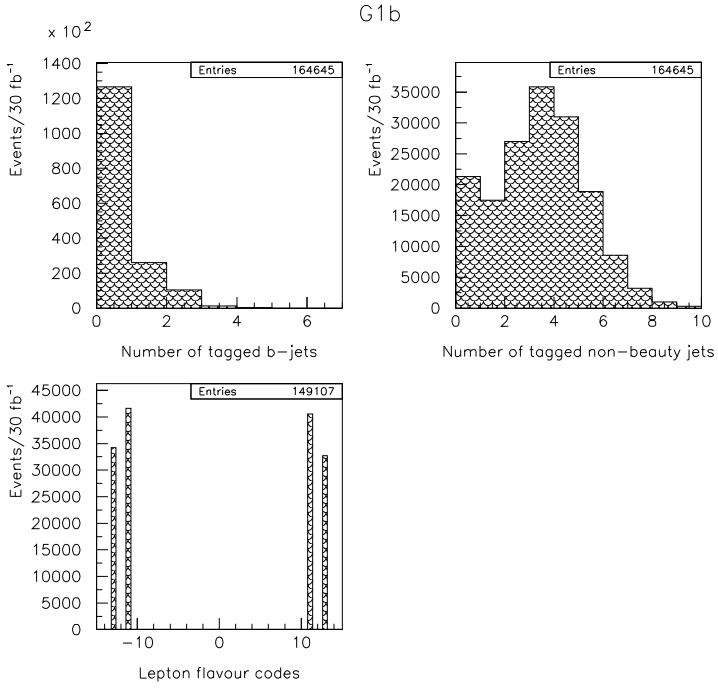

Figure 7.3: Flavour distributions at point G1b. The number of jets harder than 100 GeV. For the lepton flavour codes, 11 and 13 denote electrons and muons (respectively) and negative numbers their corresponding antiparticles.

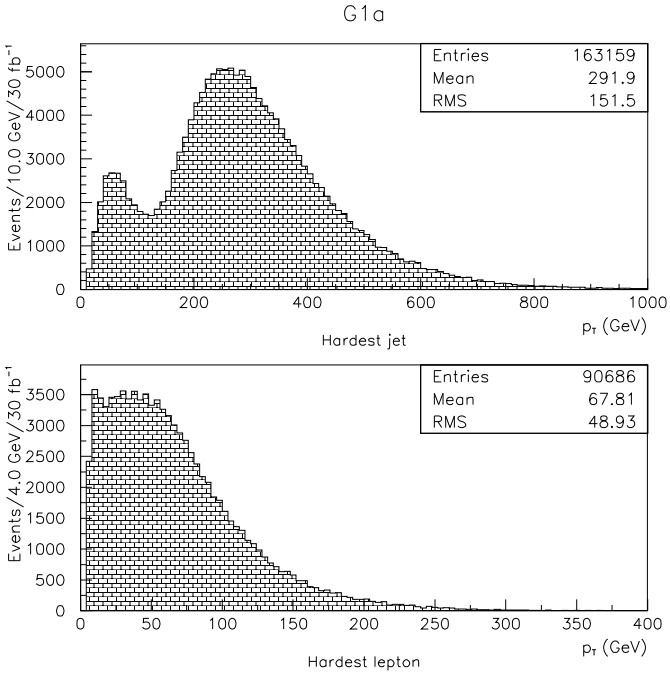

Figure 7.4: Transverse momentum distributions for the hardest jet/lepton in the event (point G1a).

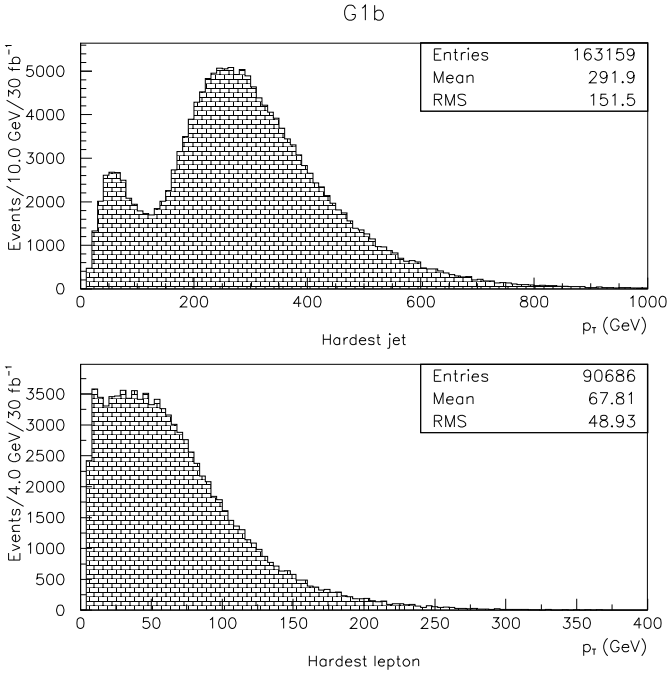

Figure 7.5: Transverse momentum distributions for the hardest jet/lepton in the event (point G1b).

We see in the two figures above that the distributions of p_T are close to identical. The main and RMS values are comparable to the ones at SUGRA point five, but the shapes of the curves are a bit different. The jets are in general softer here, but still most of them pass the signal cut on p_T.

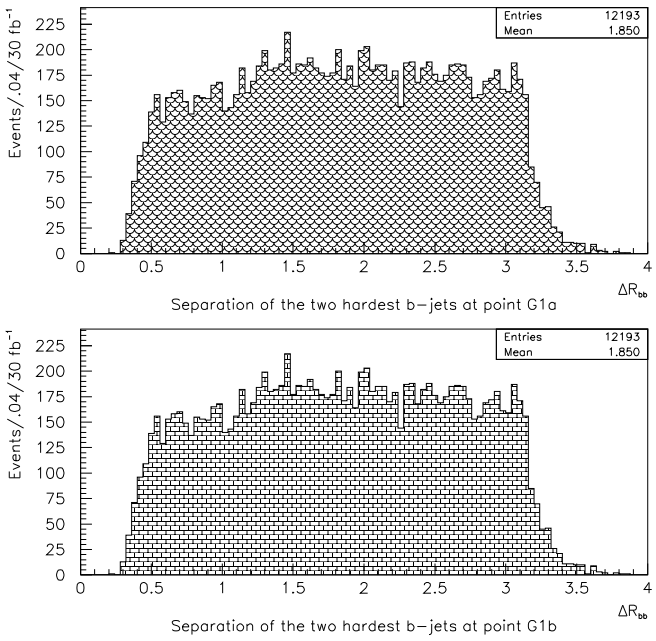

Figure 7.6: Separation of b-jets (G1a and G1b).

The low production of beauty-jets makes the top quarks significant once again; only 19% of the b-jets are below 1.0 in separation. The top quarks are mainly coming from $\tilde{q}_L \to \tilde{\chi}_2^0 q$.

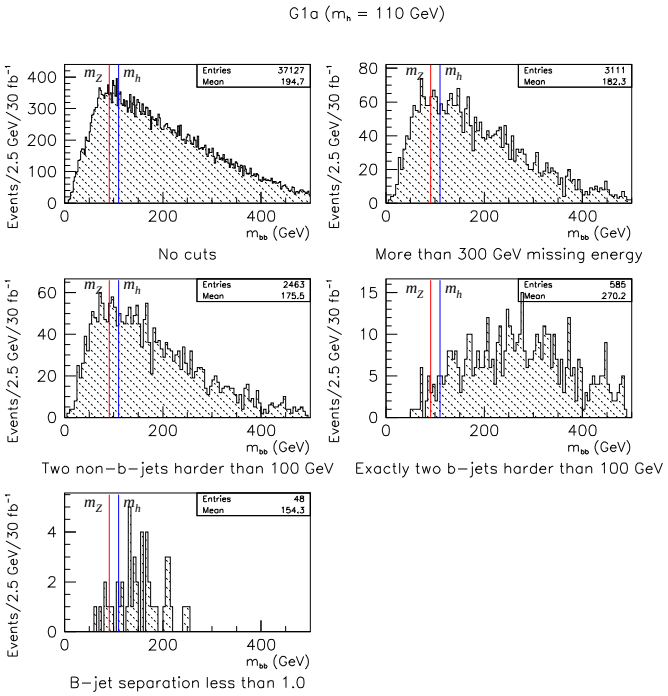

Figure 7.7: Invariant mass of b-jets, cut by cut (G1a).

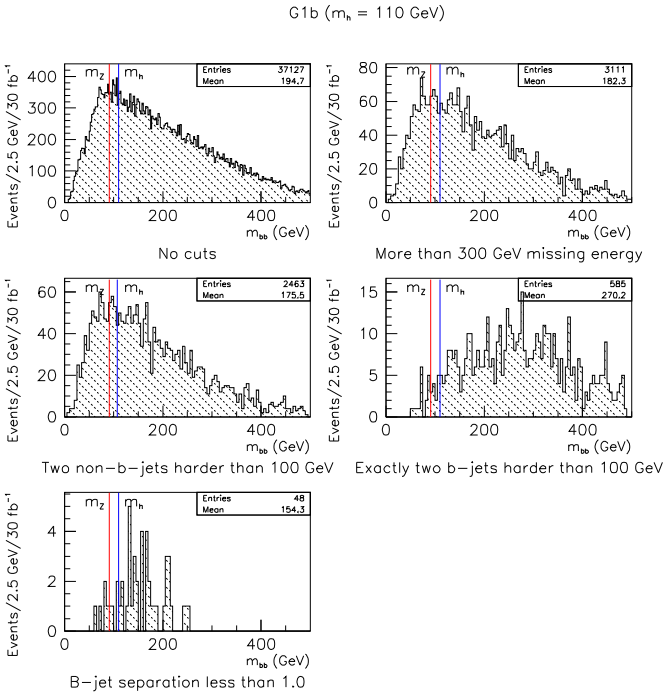

Figure 7.8: Invariant mass of b-jets, cut by cut (G1b).

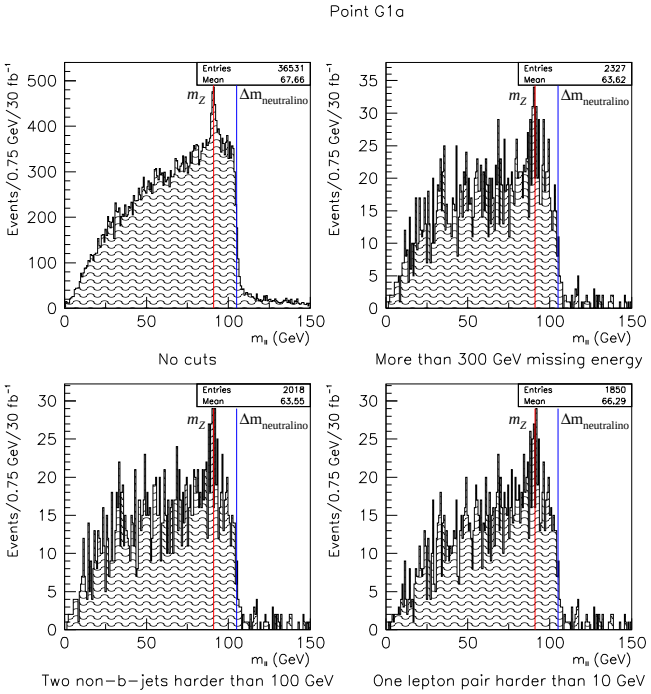

Figure 7.9: Invariant mass of lepton pairs, cut by cut (G1a).

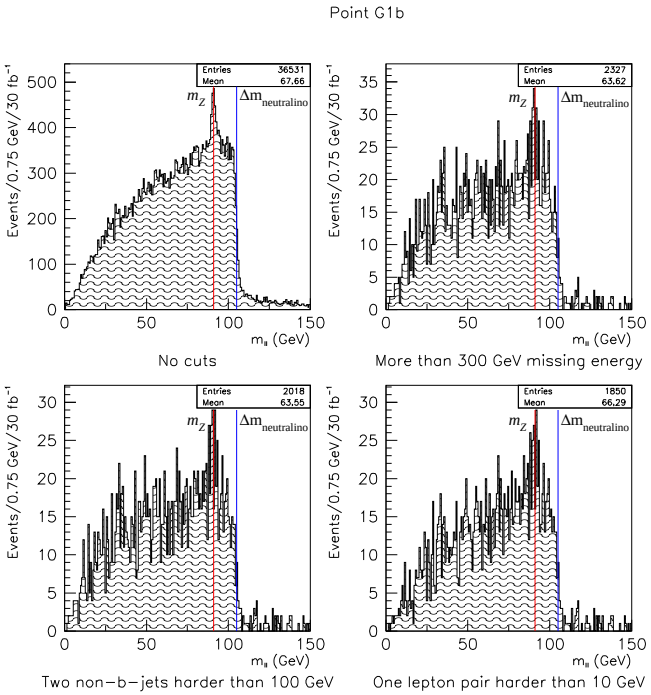

Figure 7.10: Invariant mass of lepton pairs, cut by cut (G1b).

The small number of tagged b-jets in the upper part of figures 7.7 and 7.8 is probably due to the decay mode $\tilde{\chi}_2^0 \to \tilde{\chi}_1^0 Z^0$, $Z^0 \to b\bar{b}$. In figures 7.9 and 7.10, most of the signal is from $\tilde{\chi}_2^0 \to \tilde{l}l \to \tilde{\chi}_1^0 ll \to \tilde{G}ll\gamma$, while the small peak around the Z^0 mass is from $\tilde{\chi}_2^0 \to \tilde{\chi}_1^0 Z^0$, $Z^0 \to ll$.

In the two last histograms we also see clearly the striking resemblance with SUGRA point five (figure 6.29). The shapes of the dilepton mass signals are almost identical. The main difference resides in the slightly higher kinematic edge at the neutralino mass difference at SUGRA point five.

Flavour-subtraction would probably make the small peak from Z^0 decays more distinct, removing some leptons that are not flavour correlated, which is a requirement in the channels studied in the GMSB models.

With sufficient luminosity we would be able to measure the ratio of the cross section for the neutral vector boson decay mode to the cross section for the slepton decay mode, to get information on the Higgsino content of the lightest neutralinos.

7.2 GMSB Points G2a and G2b

At points G2a and G2b all squarks are lighter than the gluinos, and the stau slepton is the NLSP. But because the mixing between the stau and the first two generations of sleptons is small, the right-handed selectrons and smuons are not allowed to decay through $\tilde{l}_R^{\pm} \to \tilde{\tau}_1 \tau l^{\pm}$. And the channel $\tilde{l}_R \to \tilde{\tau}_1 \nu_\tau \nu_l$ is suppressed compared to gravitino decays, because it is only allowed through left-right mixing terms proportional to the lepton mass. So the right-handed selectrons and smuons are so-called ‘co-NLSP’s together with the $\tilde{\tau}_1$. The three co-NLSPs will decay rapidly ($c\tau_0 = 52$ μm) into the LSP (the gravitino) in the tracker volume.

The reason why the histograms in this subchapter have higher values on the y-axis (number of events) than the ones in the previous subchapter is that the squarks are lighter at point G2a and G2b, so the total SUSY production cross section becomes a factor three larger (table 5) and the number of detected candidates increases. Histograms in this chapter are based on 100 000 events ntuples, scaled to an equivalent integral luminosity of 30 fb^{-1} as usual.

In figure 7.11 below, we see that around 20% of the events at both points pass the missing energy cut. That is the same as for SUGRA point six, and twice as much as for points G1a and G1b.

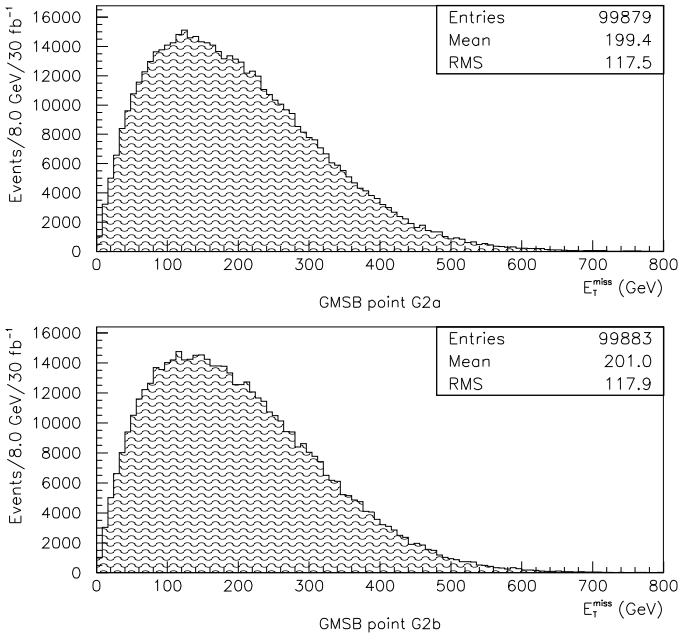

Figure 7.11: Missing transverse energy (G2a and G2b).

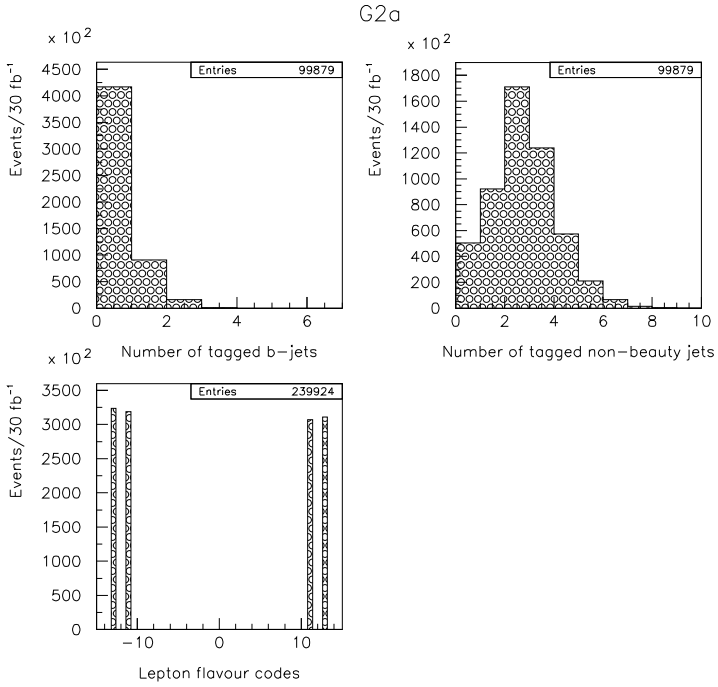

Figure 7.12: Flavour distributions at point G2a. The number of jets harder than 100 GeV. For the lepton flavour codes, 11 and 13 denote electrons and muons (respectively) and negative numbers their corresponding antiparticles.

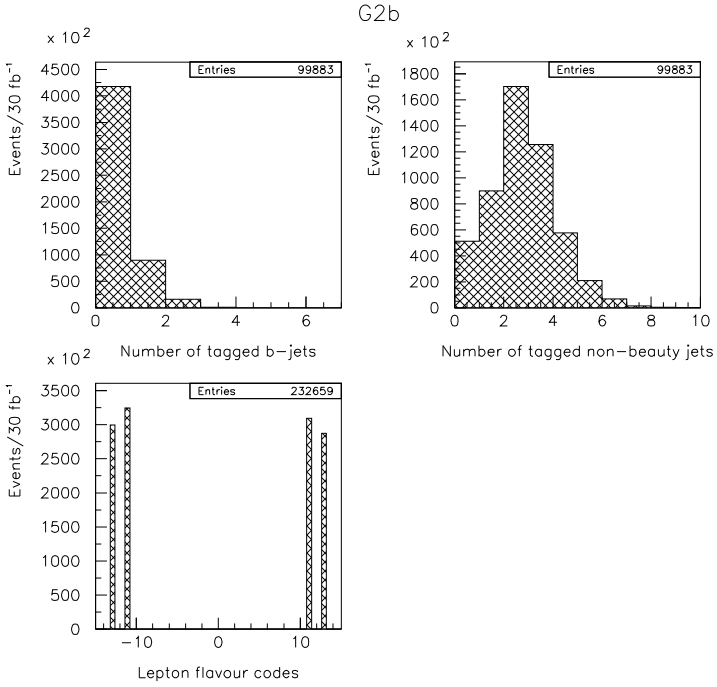

Figure 7.13: Flavour distributions at point G2b. The number of jets harder than 100 GeV. For the lepton flavour codes, 11 and 13 denote electrons and muons (respectively) and negative numbers their corresponding antiparticles.

We see that the flavour distributions are not totally identical at the two points here, as for points G1a and G1b, although the similarities are striking. Both points have hard b-jets in only 21% of the events, which is lower than any GMSB or SUGRA point, while 90% of the events have hard non-beauty jets, which is about the same as all other points (except SUGRA point three). That can be interpreted as a hint that we should not expect to see reasonable signals in the b-jet invariant mass plots in the end of this subchapter, and that the usual channels through which the b-jets have been produced in earlier chapters are probably totally closed (at least strongly suppressed).

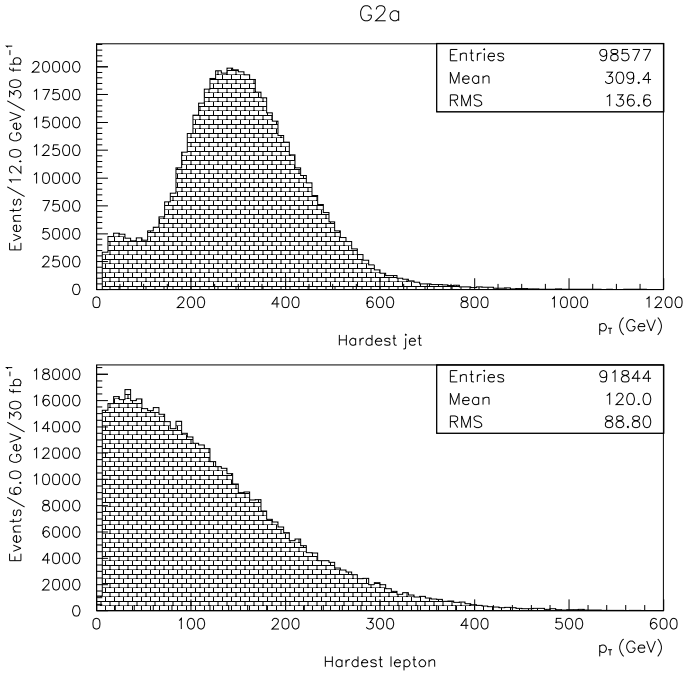

Figure 7.14: Transverse momentum distributions for the hardest jet/lepton in the event (point G2a).

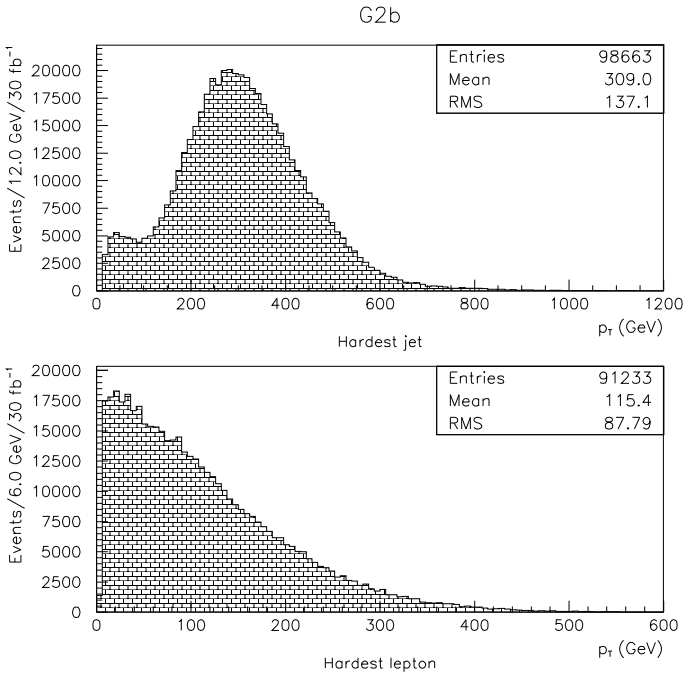

Figure 7.15: Transverse momentum distributions for the hardest jet/lepton in the event (point G2b).

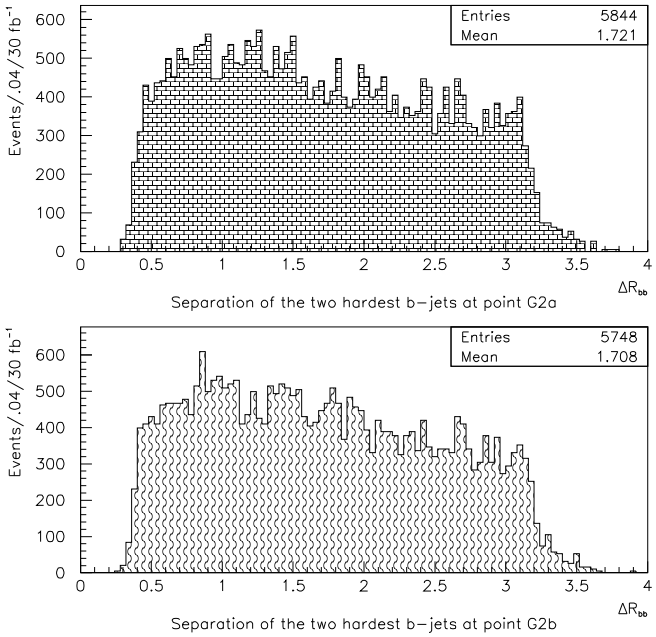

Figure 7.16: Separation of b-jets (G2a and G2b).

Considering what we found in the flavour distributions, it is not surprising to see such a low number of events in these histograms; less than 6000 events out of 100 000 SUSY events contain a pair of b-jets. And about one fourth of these pass the cut on separation, which is quite a bit above all other points that have been considered in this thesis. That means top-quarks are more rarely produced here than at the other points, which is another hint that heavy quark production is kinematically disfavoured to production of lighter quarks. Higgs decays are in other words either totally absent or at least insignificant.

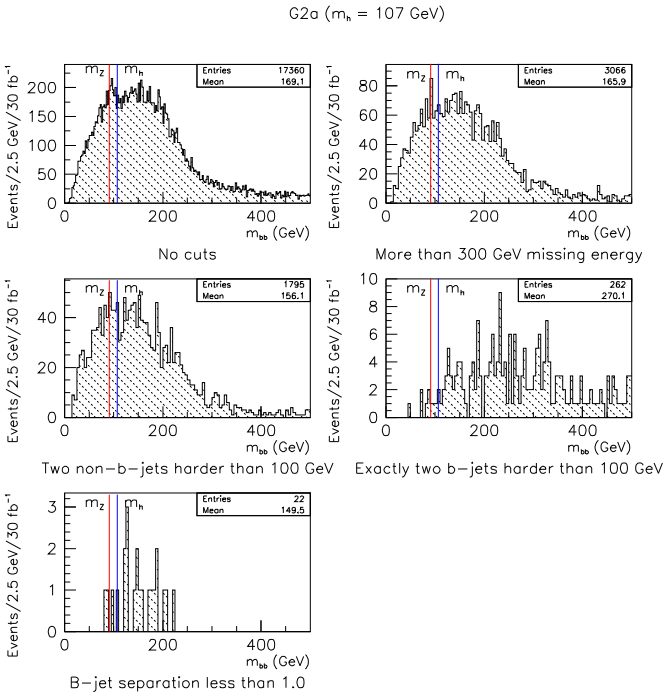

Figure 7.17: Invariant mass of b-jets, cut by cut (point G2a).

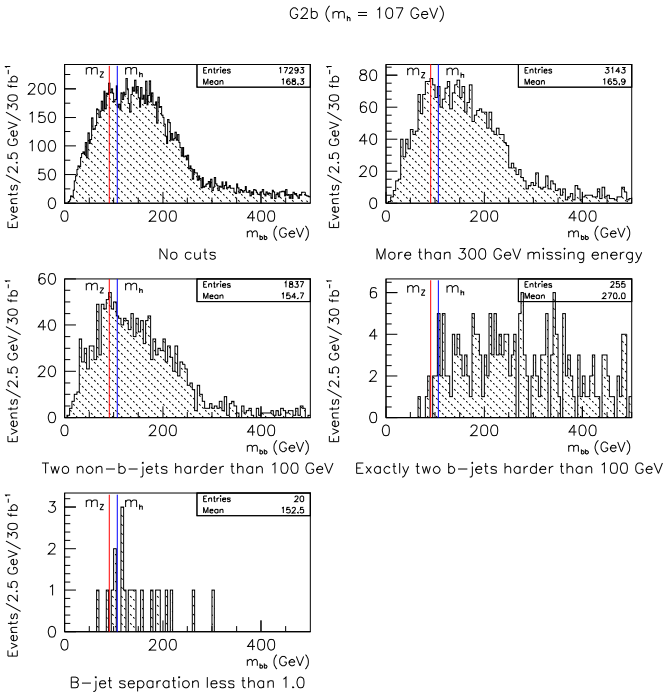

Figure 7.18: Invariant mass of b-jets, cut by cut (point G2b).

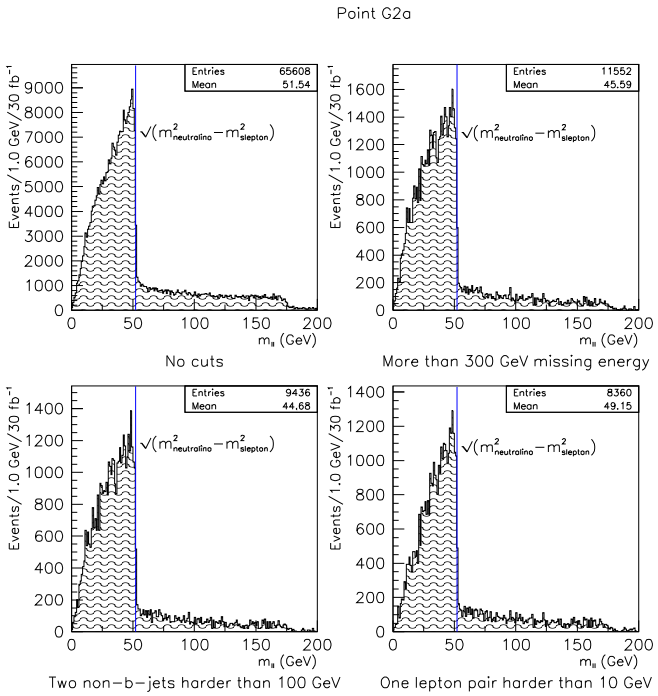

Figure 7.19: Invariant mass of lepton pairs, cut by cut (point G2a).

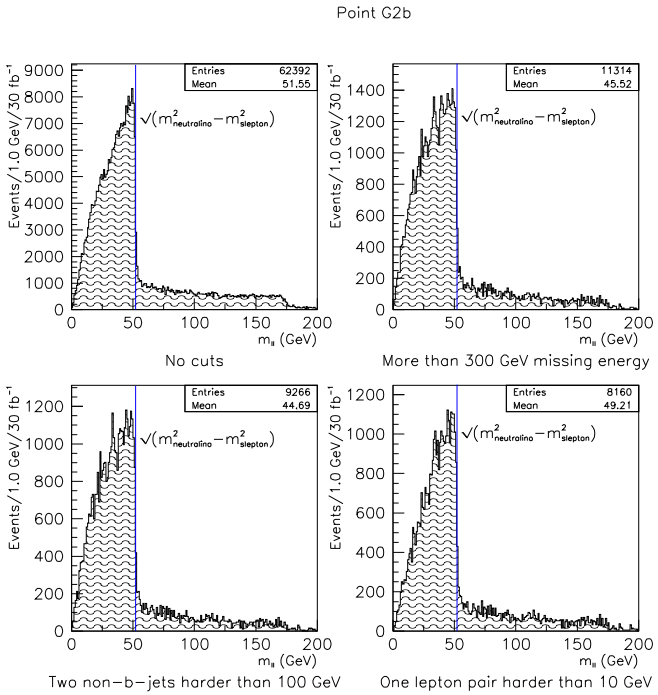

Figure 7.20: Invariant mass of lepton pairs, cut by cut (point G2b).

We see in the four previous figures that the signal is almost eliminated by the cuts. The few b-jets that are produced (through $\tilde{q}_R \to \tilde{\chi}_1^0 q \to \tilde{l} l q \to \tilde{G} l l q$, where the squarks are produced either directly or through gluino decay) are rarely hard enough to pass the cut on transverse momentum, since they appear so late in the decay chain. And the cut on separation takes away much of the signal by removing top-jet events (as usual).

The signal-like part of the dilepton mass histograms is mainly due to $\tilde{\chi}_1^0 \to \tilde{l} l \to \tilde{G} l l$, with a kinematic edge at $\sqrt{m^2_{\tilde{\chi}_1^0} - m^2_{\tilde{l}_R}} = 52.1$ GeV, while the SUSY background part is mostly from $\tilde{\chi}_2^0 \to \tilde{l} l \to \tilde{G} l l$, with an (almost invisible on a linear axis) edge at $\sqrt{m^2_{\tilde{\chi}_2^0} - m^2_{\tilde{l}_R}} = 175.9$ GeV. The edge from the decay of the second lightest neutralino is easiest identified when no cuts are imposed.

7.3 Summary

Four points have been studied in the exact same way as in the SUGRA analysis. We found that the number of beauty-jets was much smaller here, and that leptons in general play a more important role in this scenario. Similarities to SUGRA were found, especially at point G1b, where the dilepton signal is impossible to separate from the one at SUGRA point five.

The most general conclusion that enters one's mind after these studies of the GMSB phenomenology, is that the dilepton signals are in general much more promising than the b-jet signals (to a higher degree than in the SUGRA model). It is, in fact, tempting to say that we were not able to extract any new information from the dijet mass histograms. In contrast, we were able to identify a sharp endpoint from different multibody decays at all four points (even before imposing the signal cuts) in the dilepton invariant mass distributions. This strengthens the impression we had after chapter six, that studies of dilepton signals will in general (that is: in a larger part of the parameter space) allow us to learn more about SUSY than the dijet signal studies will.

In addition to the endpoints from neutralino-neutralino (G1) or neutralino-slepton decays (G2), we saw small peaks from decays of the Z^0 boson in the dilepton invariant mass histograms at points G1a and G1b. If this is found in the actual experiment, information on the Higgsino content in the neutralinos (and consequently tanβ) might be extracted, if sufficient luminosity is provided by the LHC.

Recognizing signatures from either GMSB point might tell us something about the value of C_{grav}, and thus about whether there are more contributions to SUSY breaking than just gauge mediation. This analysis, however, is not optimised for such studies.

8.0 The Background

In general, the background can be separated into reducible and irreducible, caused by Standard Model and SUSY physics. The reducible background is due to misidentification of particles in the detector, while the irreducible background is due to processes which produce the same final states as the signal.

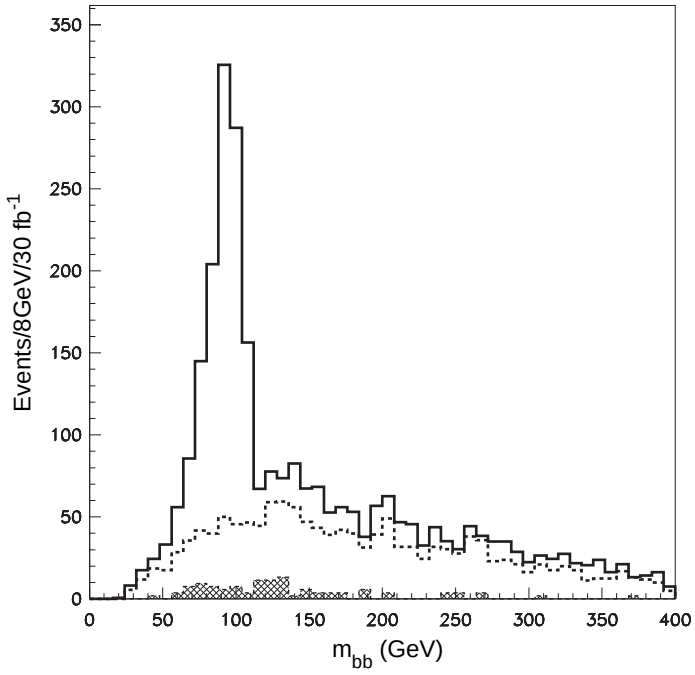

Figure 8.1: Invariant mass of two tagged b-jets at SUGRA point 1 (30 fb^{-1}). The dotted curve is the SUSY background, while the shaded histogram is the total Standard Model background (figure 20-23 from [5]).

8.1 SM Background

The Standard Model background is completely dominated by two-jet topology QCD events (both real b-jets and hadron jets misinterpreted as b-jets). The cross section is typically about a factor one to ten million larger than the total SUSY production cross section in the simulations. That makes it meaningless to generate the SM background together with the signal, because almost all the CPU time will be spent calculating SM events, and all the ntuples will after a short while be filled up with (in this context) not so interesting QCD physics.

When studying the SM background, preselection cuts on allowed minimum transverse momenta (of course less restrictive than the cuts in the analysis) were introduced in the event generator to substantially reduce the cross section. For the b-jet channel, the maximum lower limit for p_T that does not introduce an extra bias is 100 GeV (ideally a bit lower because of detector effects). For the lepton channel, the corresponding limit is only 10 GeV. This is not low enough to allow preselection cuts to make the SM cross

section small enough, although the cross section is reduced by several orders of magnitude when these limits are set higher.

Quite some effort has been made to examine how the QCD cross section is getting smaller when the minimum p_T is getting higher, but even if we make the preselection cuts several times more restrictive than the signal cuts, all we get to pass the signal cuts is a handful of events, which look like high columns when scaled up due to lacking luminosity. No reasonable shape at all, in other words.

To avoid endless simulation of SM background, I have used the ATLAS SM background studies in [5] to conclude that the SM background is much less worrying than the SUSY background.

8.2 SUSY Background

The whole SUSY cross section is generated, so all SUSY background events are automatically included in the histograms. Since the phenomenology is so different at the various parameter points, it is not trivial to point out what channels are the most disturbing to our signal definition. For instance; at most points (SUGRA one, two, five and six, as well as GMSB G2a and G2b) the gluinos are heavier than all the squarks, while in other cases (SUGRA four and GMSB G1a and G1b) it is the opposite situation.

In general, the channels $\tilde{b}_{L,R} \to \tilde{\chi}^0_{2,1} b$ give rise to b-jets that appear as an irreducible SUSY background in many of the dijet mass plots. Gluino decays are also contributing: $\tilde{g} \to \tilde{b}_1 b \to \tilde{\chi}^0_2 b\bar{b}$ (especially at SUGRA point three) or $\tilde{g} \to b\bar{b}\tilde{\chi}^0_2$ and $\tilde{g} \to q\bar{q}'\tilde{\chi}^\pm_1$ (either the quark or the antiquark being b-flavoured, the other one being "up-type"-flavoured) in cases with $m_{\tilde{g}} < m_{\tilde{q}}$.

There is no doubt that the SUSY background is of most significance in the dijet mass reconstructions. In the dilepton mass reconstructions we were able to get much cleaner signals by rejecting most of the SUSY QCD background by requiring a hard lepton pair, although we had to require two non-beauty-jets as well, because of how the neutralinos (which are parent particles for the dileptons) are produced. Cascade decays of gluinos and squarks give rise to such hard jets. At SUGRA point five and all the GMSB points the dilepton signals were actually very sharp even before the signal cuts were imposed.

9.0 Conclusions

A standard method of analysing SUSY phenomenology has been constructed, with the main purpose of reconstructing exclusive SUGRA signatures. A wide parameter space of the minimal SUGRA model is covered by Monte Carlo simulations and a fast detector simulation. Distributions of various entities are described in histograms generated in PAW.

Four points in the minimal GMSB model are also studied with the same analytical approach, using dileptons and b-jets in the final state, as these signatures are well suited for hadron machines.

It seems that we get meaningful invariant mass reconstructions even in most of the cases (that is: theoretical parameter constellations) in which the channels we are looking for are not kinematically allowed. Other channels have often appeared to fit well into the analysis. That means we will probably learn valuable things from a model dependent, channel customised analysis, even if nature chooses to serve us something very different in terms of parameters, and even to how SUSY is broken.

The studies show that the mentioned models can be explored and compared with these methods, by choosing the right final state reconstructions (in this case: b-jets and dileptons). Partial mass reconstructions are also possible in some cases, allowing us to estimate cross sections by counting events in a resonance peak, and thus put constraints upon some of the model parameters. This is not done here, but might be a natural next step in an eventual extension of these studies. The problem is that the signal is sometimes quite reduced by the cuts, so the level of precision is in general not well suited for cross section estimates.

Also, in the cases where the final states are from multibody decays, rather than the two-body decay modes upon which the analysis is built, it has been shown that an identification of the endpoint in the corresponding continous invariant mass distribution is straightforward with these methods, thus making it likely to be able to measure the mass difference of a SUSY particle in the final state and its parent particle in the actual experiment.

Concerning the aspect of deciding whether a SUSY signal fits a SUGRA or a GMSB scenario, we have learned that if we for instance see a dilepton invariant mass distribution with a shape similar to parameter points in both models (figures 6.29, 7.9 and 7.10), the resemblance between the models vanishes when we look at the dijet signal (figures 6.28, 7.7 and 7.8). That means one can just look at the b-jet mass reconstruction if the shape of the dilepton signal is ambiguous in respect to what SUSY model it supports. The opposite case is also true; similar dijet mass reconstructions (figures 6.34, 7.17 and 7.18) are found, but then there are huge differences in the dilepton signal (figures 6.35, 7.19 and 7.20). In that way one might say that studying two (or indeed several) channels instead of one is a kind of convenient security in case of ambiguous signals.

The biggest limitation of the software and hardware tools has been the lacking ability to generate a proper amount of SM background. This is a very serious problem, which is mostly due to lack of available computer resources (both disk space, CPU speed and

limitation on ntuple sizes in PAW). For future studies of the background in ATLAS, one should use the “once-and-for-all” generated SM background data which is stored on tapes at CERN. The extremely small cross section of SUSY physics compared to Standard Model physics is the reason why generating the SM background is so difficult, as discussed in chapter 8. However, the SM background’s impact on the signal reconstruction is almost negligible (illustrated in figure 8.1). Other SUSY processes are dominating the background, and those are generated together with the signal without any difficulties. Still, the lack of background studies is the biggest weakness of this analysis.

It is natural to ask the questions: “Why look for these final states, when different SUGRA and GMSB points provide different signatures?” And: “Why apply an analysis customised to SUGRA points one and two to all the other points and GMSB as well?”. The answers are as follows: Firstly, dileptons and b-jets are very clean signatures in a hadron collider environment, sharply distinct from most backgrounds. The reconstruction is also somewhat compatible to several other signature reconstructions at other points. Secondly, why not? A similar analysis could just as well have been made, customised to a different decay mode, favoured by a different parameter point. Maybe even by GMSB. In any case, we do not know what nature will provide at the LHC startup. So we would better decide a way to sort out the data, and agree to what we will be looking for, and thus be prepared to find something quite different than what is ideal for our methods (which is obviously the most likely outcome no matter what approach we make).

There is obviously an enormous amount of phenomenological aspects left to prepare by similar simulation studies. It has been a goal in these studies to try to draw some lines throughout the SUGRA and GMSB parameter spaces, to keep the analytical approach on a somewhat general and qualitative level, although two specific decay modes, favoured by only a few parameter points, were designated starting-points. For future projects of further examinations of SUSY phenomenology in ATLAS, it is recommended to make the extra effort of applying the method of the specific analysis on other parts of the parameter space than what is believed to be the most promising, as well as including competing models (SUGRA, GMSB and AMSB [11] are all available in the latest versions of ISAJET). This recommendation is given not only of general reasons, but also because in my case, this way of doing it gave a surprising amount of physics signals beyond what was expected and searched for in the first place. It may also be interesting to construct a more statistical method, to acquire more quantitative information on the SUSY discovery potential in ATLAS, given a certain model.

10.0 References

[1] http://public.web.cern.ch/Public

[2] Numerical recipes in FORTRAN77: The art of scientific computing (ISBN 0-521-43064-X), Cambridge University Press

[3] http://cern.web.cern.ch/CERN/Experiments.html

[4] ATLAS Physics Technical Design Report Volume I

[5] ATLAS Physics Technical Design Report Volume II

[6] ISAJET 7.48, Frank E. Paige and Serban D. Protopopescu, Physics Dept., Brookhaven National Laboratory, USA, Howard Baer, Dept. of Physics, Florida State University, USA, Xerxes Tata, Dept. of Physics and Astronomy, University of Hawaii, USA

[7] ATLFAST 2.0, Elzbieta Richter-Was and Daniel Froidevaux, CERN, Luc Poggi-oli, LPNHE, France

[8] http://pdg.lbl.gov/atlas

[9] http://suite101.com/article.cfm/advanced_physics/19964

[10] The Data Analysis BriefBook (the Internet version), R.K. Bock and W. Krischer at CERN (http://www.cern.ch/RD11/rkb/AN16pp/node177.html)

[11] “Phenomenological consequences of supersymmetry with anomaly induced masses”, Tony Gherghetta, Gian F. Giudice and James D. Wells (hep-ph/9904378)

[12] http://atlasinfo.cern.ch/Atlas/ATLASFIGS/atlasfigures.html

[13] The PAW manual

[14] http://sg1.hep.fsu.edu/~blessing/talk/cern/slides/tsld003.htm

[15] http://rd11.web.cern.ch/RD11/rkb/PH14pp/node146.html#145

[16] ATLAS Technical Proposal

[17] Physics Letter B260 447 (1991), U. Amaldi, W. de Boer, and H. Furstenau

[18] Internal seminar on MSSMs in Oslo, March 2001, Finn Ravndal, Physics Dept., University of Oslo, Norway

[19] “Tesla: What is it and why do we need it?”, talk given by D.J. Miller (DESY) at the Dept. of Physics, University of Oslo, March 2001

[20] P. Igo-Kemenes (Heidelberg/CERN), “Status of Higgs Boson Searches” (LEP Seminar), 3. November 2000